Title: Income strongly moderates climate-driven migration

Authors: Gaurav Khanna1†, Pascal Polonik1,2,3, Jessica S. Wan2,4, Jacopo Lunghi5,6, Ida Grigoryeva7, Katharine Ricke1,2∗†

1 School of Global Policy and Strategy, University of California San Diego, La Jolla & 92093, USA.
2 Scripps Institution of Oceanography, University of California San Diego, La Jolla & 92093, USA.
3 Doerr School of Sustainability, Stanford University, Stanford, CA, USA.
4 Climate Systems Engineering initiative, The University of Chicago, Chicago, IL, USA.
5 CMCC Foundation - Euro-Mediterranean Center on Climate Change, Italy
6 RFF-CMCC European Institute on Economics and the Environment, Italy
7 Department of Economics, University of California San Diego, La Jolla & 92093, USA.
∗Corresponding author. Email: kricke@ucsd.edu

Income strongly moderates climate-driven migration

Gaurav Khanna[1†], Pascal Polonik[1,2,3], Jessica S. Wan[2,4]

Jacopo Lunghi[5,6], Ida Grigoryeva[7], Katharine Ricke[1,2*†]

[1]School of Global Policy and Strategy, University of California San Diego, La Jolla & 92093, USA.

[2]Scripps Institution of Oceanography, University of California San Diego, La Jolla & 92093, USA.

[3]Doerr School of Sustainability, Stanford University, Stanford, CA, USA.

[4]Climate Systems Engineering initiative, The University of Chicago, Chicago, IL, USA.

[5]CMCC Foundation - Euro-Mediterranean Center on Climate Change, Italy

[6]RFF-CMCC European Institute on Economics and the Environment, Italy

[7]Department of Economics, University of California San Diego, La Jolla & 92093, USA.

[*]Corresponding author. Email: kricke@ucsd.edu [†]These authors contributed equally to this work.

Understanding how climate change will reshape human migration remains an open empirical challenge. Migration decisions reflect a complex interplay of environmental and socioeconomic factors, yet existing data and models have struggled to capture this interaction at a global scale. To address this, we assemble spatially granular, long-panel migration data covering nearly the entire world and develop a statistical model that captures how both climate and income dynamics shape rural-to-urban migration responses. Using this new approach, we uncover a strong and robust dependence of climate-driven migration on income levels, as well as a nonlinear relationship between internal migration and climate. We then use these relationships, together with international migration data, to project how migration pressures will be shaped by the interaction between warming and income growth. Our findings show that the magnitude and geography of climate-induced migration will depend critically on how quickly incomes rise across the world.

Prospects for climate-driven human migration, while potentially of significant consequence for societies and policymakers, remain difficult to project (*1, 2*). This challenge stems both from the complexity of migration decisions (shaped jointly by environmental shocks and income opportunities) and from the lack of harmonized, spatially granular data tracking migration over time and across the globe (*3–5*). Climate change can alter migration patterns by reshaping local economic opportunities, agricultural productivity, and living conditions (*6–8*). Yet, there may be substantial heterogeneity in these responses across settings, reflecting variation in both climatic exposure and the capacity to adapt or move (*9–12*).

Prior research has documented nonlinearities in temperature–migration relationships (*13, 14*), income dependence in climate sensitivity (*8, 15, 16*), and larger responses in rural settings (*17–19*). Different lines of work have provided these insights through varying lenses: some analyzing specific countries or regions, others using coarser spatial units or shorter time horizons, and still others offering global correlations or projections (*20, 21*). Each of these perspectives sheds light on part of the overall relationship between climate and migration, yet these insights have typically been examined separately. Here we combine these elements in a comprehensive framework, assembling spatially granular migration data that span nearly the entire world and developing a long-run panel model that captures within-location variation over more than four decades. Our model focuses on internal, predominantly rural-to-urban migration, which serves as a key channel through which climate pressures manifest and accumulate within countries (*15, 22*). Given the heterogeneity in these responses across income levels and the structure of existing cross-border migration links, this framework provides a comprehensive global analysis that connects internal movements to international migration pressures and enables projections of how global migration pressures may evolve under warming and income-growth scenarios.

Recent data efforts have produced spatially resolved hindcasts of net migration in 5-year intervals using a combination of satellite and census data, yielding the most consistent and transparent global migration estimates to date (*5*). For the following analysis, we carefully partition rural observations (see Materials and Methods), focusing on rural-to-urban migration for two reasons. First, the literature shows that rural communities are substantially more climate sensitive (*8, 17, 23*). Second, urbanization has been the dominant form of internal migration over the past century (*24, 25*), so even small climate-driven shifts in rural-to-urban flows translate into a large share of total climate-

induced movement. Because this type of migration dwarfs other forms of internal migration at the global scale, it provides a natural starting point for quantifying overall climate-driven migration pressures. Our dependent variable, rural out-migration, is derived directly from net migration estimates. We interpret changes in net migration for rural locations as changes in rural outflows, an assumption justified by the overwhelming dominance of rural-to-urban moves relative to urban-to-rural moves across most of the world over the past half-century (*24–26*). We exclude all observations corresponding to urban areas, thereby setting aside urban-to-urban mobility, the other major component of internal migration.

We develop a two-stage analytical framework to project future internal and international migration pressures (Fig. 1). First, we estimate income-dependent relationships between climate variations and rural-to-urban migration over 5-year intervals using panel data on historical grid-cell rural migration rates (*5*), matched to grid-cell climate (*27, 28*) and income measures (*29*). We then apply these estimated historical relationships to climate projections (*30*) for the coming decades to construct grid-cell level forecasts of climate-driven rural out-migration. Second, we use panel analysis of harmonized international survey data (*31*) to quantify how country-level internal migration patterns shape international emigration. These estimated linkages are embedded within a source–receptor model (*32, 33*) to project changes in international migration pressures under scenarios that both exclude and incorporate future income growth.

Income as the dominant moderator of climate-driven migration

We find a strong inverted-U-shaped income gradient in the relationship between climate variation (temperature and precipitation) and rural out-migration. While prior studies on rural–urban migration (*15*), cross-border migration (*34*), and internal rural mobility (*35*) have each documented versions of this inverse-U pattern, these insights have largely emerged from specific national or regional contexts. Our analysis provides the first comprehensive and globally consistent evidence that this relationship is a universal feature of climate-driven migration. This pattern implies that climate-driven emigration peaks among middle-income populations. Low-income households often lack the liquidity to finance migration and can become "trapped" in place when adverse conditions intensify (*10, 11*). Middle-income households have both the resources to move and livelihoods that

remain vulnerable to climatic shifts, making them the most responsive. High-income households, by contrast, tend to have better local opportunities, alternative adaptation strategies, and derive livelihoods less directly tied to climate-sensitive sectors (*8, 9, 36*), dampening their migration response.

In our analysis, income levels vary across grid cells, allowing us to examine how the climate–migration relationship changes across the income distribution. We find a strong inverted-U-shaped income gradient in the historical relationship between global climate variation (temperature and precipitation) and rural out-migration (Fig. 2A-B). Accounting for these nonlinear interactions between climate and income is essential for identifying the climate effects on rural-to-urban migration. In contrast, models that include temperature and precipitation alone, or only linear interactions with income, yield effects that are neither consistent nor statistically significant ($p<0.05$) (Table S3).

In the inverse-U-shaped relationship between temperature-induced rural out-migration and income (Fig. 2A), migration rates peak among middle-income groups that may have more financial resources to migrate and be economically exposed to rising temperatures. A similar pattern emerges for precipitation changes (Fig. 2B). We control for the underlying, climate-independent association between rural out-migration and income in our estimation, but omit it from the projections (see Materials and Methods), as the causal direction between income and migration is inherently ambiguous, and our objective is to isolate the climate-induced component of migration.

We project future changes to internal migration for several prominent countries in the temperature–income space (Fig. 2D), with arrows indicating projected changes under the SSP2-4.5 "middle-of-the-road" scenario. India, for example, currently experiences high temperatures and is middle-income; further warming is likely to increase rural emigration, and the amount of income growth expected over the next 25 years exacerbates this effect. In China, warming likewise increases emigration, but rising incomes expand adaptation options as China's baseline income has already surpassed the income at which migration rate peaks. Unlike in India, rising incomes in China are therefore expected to reduce climate-driven rural out-migration. Rising incomes also dampen the sensitivity of rural out-migration to precipitation changes (Fig. 2E).

By contrast, and consistent with both the construction of the dataset and dominant migration patterns over the past four decades, climate-driven migration in urban areas follows an inverse, but statistically weaker relationship than in rural settings (Table S6, Fig. S6). Temperature-driven urban

in-migration also reaches its minimum at middle incomes, reflecting urbanization as an adaptation response to rural climate shocks.

Climate's signature in historical rural migration

After controlling for nonlinear income dependence, we find that – while sensitivities vary – warmer and dryer conditions are associated with higher rural outmigration rates (Fig. S7). The effects of temperature and precipitation on rural out-migration are highly significant ($p<0.01$) (Table S3). We test the global temperature relationship identified by our preferred specification at the grid cell level (akin to (*37*)), and find that the global and local linear slopes are statistically indistinguishable for approximately 78% of grid cells (Fig. S8), and at least 72% of grid cells on all continents (Fig. S9).

While in most places warmer temperatures drive higher emigration rates, the dependence is nonlinear. The marginal effect of additional warming varies substantially by income, with higher sensitivity for rich locations at high temperatures and poor locations at low temperatures (Fig. 2D, Fig. S7A). Contrary to the rest of the world, in the poorest, hottest places, each warmer five-year period dampens migration, possibly driven by the high damages of heat shocks in the most climate vulnerable societies (*38*), likely restricting households' ability to finance moves. We note that climate-driven migration in our 45-year study period has occurred in the context of a universally warming climate (Fig. 2C), making our findings challenging to disentangle from lower frequency (multidecadal) variability.

Precipitation-driven rural out-migration likewise exhibits a robust nonlinear income dependence (Fig. S7B), but we do not identify any significant nonlinearity in the relationship between precipitation itself and migration. Drier conditions are associated with higher rural out-migration in both the highest and lowest income locations and a small but statistically insignificant decrease at middle incomes (Fig 2E, Fig S7). Unlike temperature, rural locations in the dataset experience a more heterogeneous range of low-frequency changes to precipitation, both wetting and drying over the study period (Fig. 2F).

Because migration decisions often unfold over time and individuals may not relocate in response to a single short-lived shock, we view a five-year period as a reasonable interval of analysis. Moreover, globally consistent, spatially resolved migration data are typically unavailable at shorter

timescales, making the five-year focus both practical and conceptually appropriate. In order to investigate whether five-year mean temperature and precipitation are sufficient climate metrics for migration analysis, the explanatory power of additional measures of climate and climate change were tested in alternative model specifications (see Materials and Methods). Measures of the rate of temperature and precipitation change (i.e., trend) and the volatility of climate state (i.e., variability) were generated from the same environmental observations (*27, 28*) (Fig. S5). While we find that in some cases the rate of change or the higher frequency variability to have a statistically significant relationship with rural out-migration (Fig. S11), the magnitude of the effect of changes to these variables on projected future rural out-migration is minimal compared to the effect of five-year mean temperature or precipitation. To take an agnostic approach to variable selection in the face of extensive model specification options, we also applied a LASSO variable-selection approach to select and test the implications of alternative model specifications (see Materials and Methods). We found that LASSO-generated models considering a wider selection of climate metrics and their linear combination did not provide additional power or substantially alter the projections relative to the more parsimonious and interpretable model we present here (Fig. S2).

Using our model of historical climate migration, climate model output, and gridded estimates of future income, we apply a Monte Carlo approach to project future climate-driven migration that accounts for empirical climate and statistical model uncertainties under four Shared Socioeconomic Pathways (SSP1-2.6, SSP2-4.5, SSP3-7.0, and SSP5-8.5). See Materials & Methods; see Supplementary Text.

Projections using fixed 2015 income levels consistently show an increase in climate-driven rural out-migration nearly everywhere (Fig. S10A, Fig. 4A) with the largest changes and uncertainty associated with the higher warming pathways (SSP3-7.0 and SSP5-8.5). Because many locations are already near or beyond the income at which warming-driven migration is maximized, including income growth, reduces climate-induced rural migration (Fig. S10B) in much of the world. In this income-varying case, the largest changes and uncertainty associated with the high growth pathways (SSP1-2.6 and SSP5-8.5) illustrate the dominance of income in determining climate-driven rural migration pressures (Fig. S10B).

Robust increases in rural out-migration are concentrated in relatively few countries in parts of Africa and Asia (Fig. 4B). Most countries are projected to have substantial decreases in rural out-

migration when both climate and income are allowed to vary. This includes wealthier regions—such as North America and Europe, but also parts of China, Indonesia, Latin America, and South Africa, which all experience lower out-migration as higher incomes facilitate alternative adaptation strategies. By contrast, sub-Saharan Africa, the Middle East, and Central Asia continue to exhibit high rates of rural–urban migration. In these regions, projected income growth from low to middle levels increases households' ability to finance migration while livelihoods remain highly climate-sensitive, thereby sustaining elevated migration flows (*8*). Consistent with our finding of income as the driving moderator of climate-driven migration, the magnitude of migration rate is generally much larger when using time-varying income projections. Since global and local economic growth vary by socioeconomic scenario, the timing and magnitude of projected changes is sensitive to the choice of SSP (Fig. S10B).

Cross-border migration pressures

Changes in rural–urban migration are also likely to generate migratory pressures across national borders. Increased internal mobility can exacerbate urban stresses, which in turn may spur greater emigration abroad. To examine these dynamics, we use the IPUMS International database (*31*), which harmonizes census and survey data from 43 countries over 1985–2017 (see Materials and Methods). Country-level internal migration is strongly and significantly associated with subsequent international migration pressures (Fig. S3). To project the likely destinations of these emigrants, we draw on historical bilateral migration patterns (*32, 33*). Combining these steps allows us to illustrate that the geographic distribution of future migratory pressures worldwide will depend strongly on economic development trajectories (Fig. 4C–F). We characterize our projected changes in international migrants and associated increases or decreases in migration "pressures," recognizing that strong and adaptive policy constraints on international immigration mean that even where motivation to migrate exists, feasible pathways may not.

Keeping income levels constant, China emerges as a major sending country (due, in part, to its large population), with roughly 819,000 projected migrants over each 5-year period (Fig. 4C, Table S7). However, when income growth is incorporated (Fig. 4D), China's projected emigration declines sharply, consistent with the idea that rising incomes facilitate alternative adaptation strate-

gies and reduce climate sensitivity. By contrast, out-migration pressures from India and several sub-Saharan African countries increase markedly, driving a heightened likelihood of cross-border migration. Under SSP2-4.5, in 2050, average income in rural India is projected to be close to those associated with peak climate-driven migration. We project that in 2050, in India alone out-migration pressure increases by about one million migrants every five years.

Reflecting its historical role as a primary destination for migrants from Latin America and China, the United States shows the largest projected increases in inflow pressures when incomes are held constant (Fig. 4E), receiving roughly 432,000 climate migrants every 5 years. Yet when income growth is incorporated (Fig. 4F), U.S. border pressures diminish meaningfully, as many key sending countries may adapt through non-migration strategies or experience reduced climate dependence. In contrast, intra-African migration pressures intensify, with several African countries projected to experience increased inflow pressures from neighboring states experiencing rising emigration rates.

Discussion

A wide range of regional, location-specific studies have documented a nonlinear relationship between climate, migration, and income. Our analysis demonstrates that this pattern is both robust and universally consistent, revealing income as a central moderator of climate-driven migration. Across the world, and in response to both thermal and hydrological stress, migration emerges as an adaptation strategy that individuals pursue when they have the means to do so, but tend to forgo once they become sufficiently affluent.

The global gridded migration dataset we examine is the product of high-resolution satellite observations of the built environment combined with national and subnational administrative unit census-based measurements (*5*). Unlike previous gridded migration datasets (*3,4,39*), the analytical approach applied in its construction was formulated with the goal of promoting the analysis of climate migration and urbanization at a high spatial resolution (*5*). Nonetheless, this imputed dataset is best suited for examining globally generalizable features of the relationship between migration patterns and climate, not for making precise local projections. The advantage of such a gridded global dataset, over more precise local or aggregate measures, is that it makes feasible an

analysis that exploits the heterogeneous climate variability associated with the entirety of human settlements. In recognition of the potential limitation of using grid-cell-level migration data that rely on imputation methods, we conduct numerous robustness checks that provide confidence in our findings. For instance, even with standard errors clustered conservatively at the country level, the fundamental relationships identified between rural migration rates and temperature, precipitation, and income are robust (Table S5).

While we present a comprehensive framework for understanding the interdependencies between local, national, and international migration pressures, the estimates we present are incomplete. We do not account for other important types of climate migration, in particular, expected changes to forced migration from large disasters such as stronger tropical cyclones or floods. To the extent that evidence about and projections of these types of migration can be generalized, and established as independent from economically driven rural-to-urban migration, other forms of climate-driven migration can be readily incorporated into our larger framework to understand how they may counteract or amplify each other.

Our estimates suggest that climate-driven international migration is likely to rise by several hundred thousand people a year – a relatively small share of global migration, but still meaningful for the regions where these pressures will concentrate. The pattern is regionally heterogeneous: as countries move from low to middle incomes, particularly in parts of Africa and Asia, they become more sensitive to climate stress, and contribute more to cross-border migratory pressures. Other countries may see pressures ease as incomes and adaptation capacity grow. Taken together, these projections show that the trajectory of climate-driven migration will depend as much on economic development as on warming itself. This underscores the need for policies that strengthen adaptation and reduce vulnerability, particularly in emerging economies, and that manage cross-border mobility proactively, including through viable legal pathways in places where climate pressures are expected to intensify.

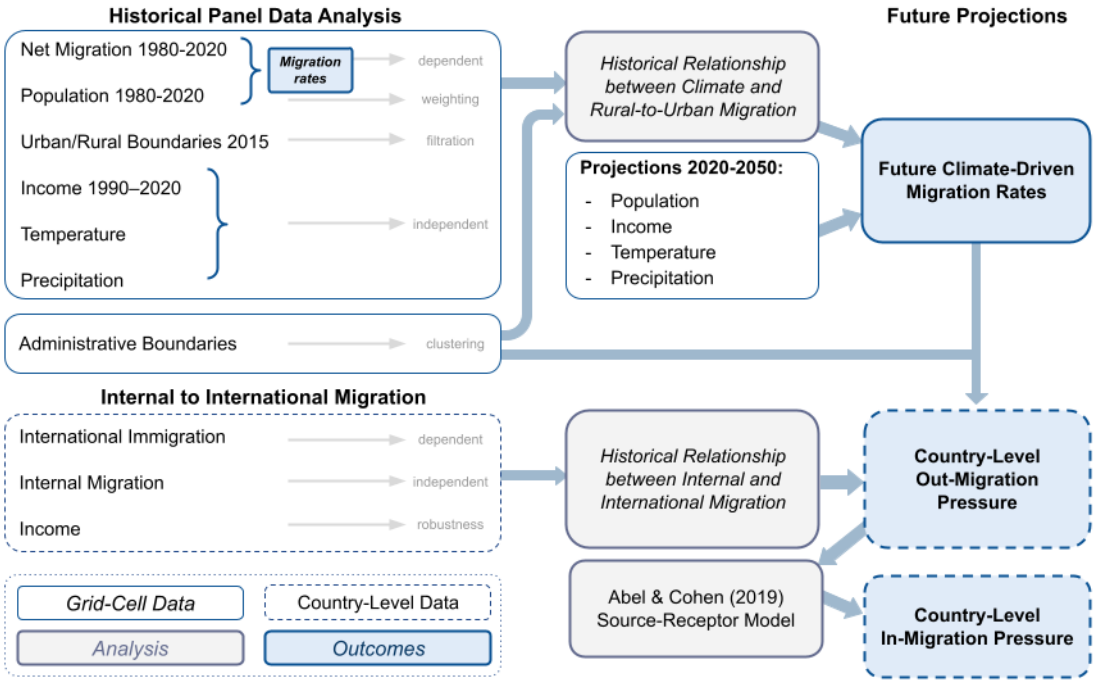

Figure 1: **Schematic of Data Sources & Processing.** We assemble a global grid-cell panel (1980–2020) with net migration, population, 2015 urban–rural boundaries, per-capita income (1990–2020), temperature, and precipitation, using administrative boundaries for clustering. We then combine these data with several sources of administrative boundaries to maximize global coverage of subnational units across countries to construct the panel data at the main unit of analysis: grid cell by administrative region. These data identify the historical relationship between climate and rural-to-urban migration via fixed-effects econometric models with income interactions (Materials and Methods). Using the estimated historical relationships from the econometric model and combining them with projections for 2020–2050 of population, income, temperature, and precipitation, we generate future climate-driven internal migration rates at the grid-cell level. In the lower part of the figure, we describe how an auxiliary specification links internal migration to international immigration using country-level data on immigration and income, and a source–receptor accounting of bilateral flows to translate grid-cell movements into country-level out-migration and in-migration pressure (based on Abel and Cohen flow matrices (*32, 33*)). White boxes denote data inputs (solid outlines for grid-cell data and dashed boxes for country-level data). Gray boxes denote analysis steps, and blue boxes denote derived model estimations and projection output. Blue arrows trace the flow of our empirical estimations and projections modeling: from historical estimations to capture the historical relationship between climate and migration to future projections, with additional analyses aggregating our grid-cell level data to country-level estimates. See Materials and Methods for data sources, variables, and the full model specifications.

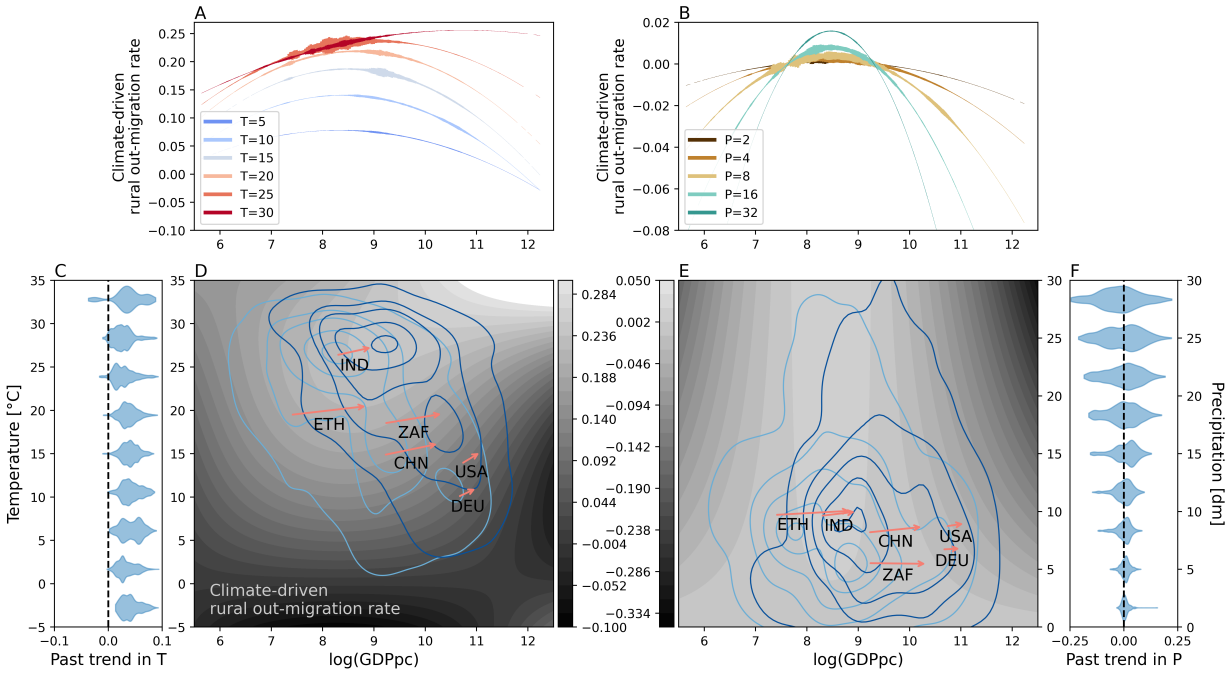

Figure 2: **Empirical characterization of climate-driven migration.** Climate-driven rural outmigration rate shown as a function of log(GDPpc) and temperature (**A**) and precipitation (**B**) in color. Line width indicates the number of historical observations in the bin. Joint climate and log(GDPpc) results are shown in shaded contours for temperature (**C**) and precipitation (**D**), with the historical and 2050 projected (SSP2-4.5) distributions shown in contour lines. The arrows indicate the change from 2015 to 2050 of select countries (China, CHN; Ethiopia, ETH; Germany, DEU; India, IND; South Africa, ZAF; the United States, USA) for SSP2-4.5. Though the absolute values differ, the range of shading is the same in (**D**) and (**E**). Lastly, we include binned histograms of trends over the observational period of temperature (**C**) and precipitation (**F**)

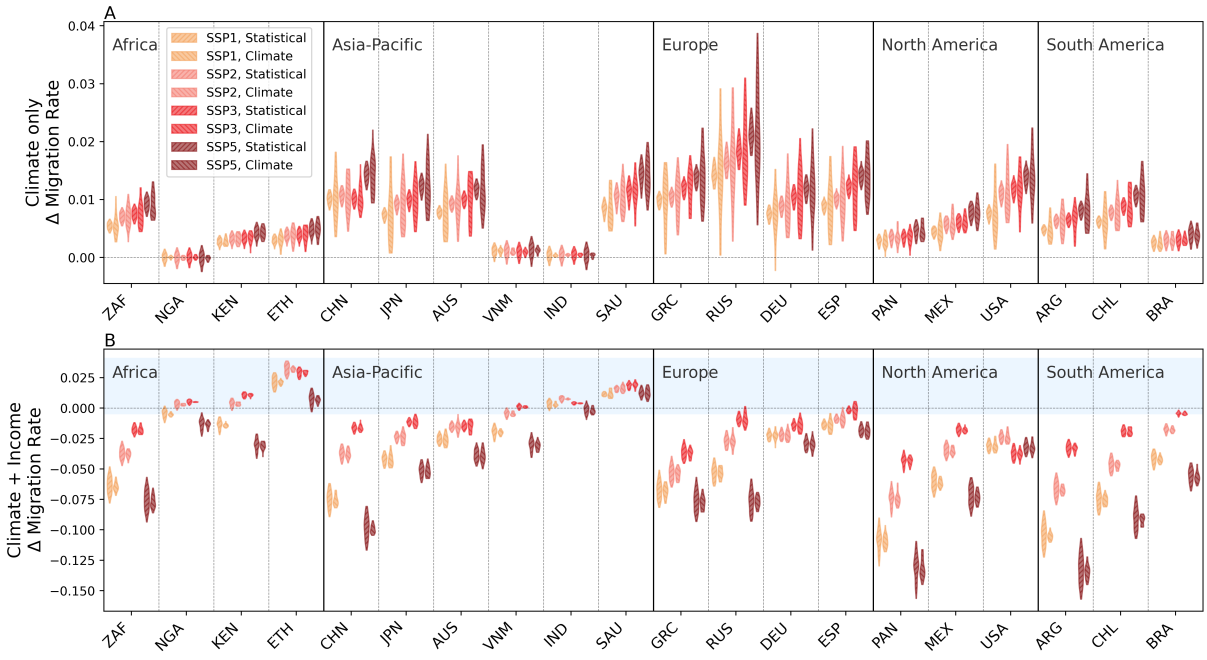

Figure 3: **Projected changes to climate-driven migration rates in 2050 relative to 2015 for select countries and for different SSPs, together with the associated uncertainties.** Projections using a changing climate and fixed income are shown in (**A**), and projections using a changing climate and changing income are shown in (**B**). Shared Socioeconomic Pathways (SSP1-2.6, SSP2-4.5, SSP3-7.0, and SSP5-8.5) are designated by color. Countries are labeled with ISO 3166 codes. Uncertainty ranges are decomposed into statistical uncertainties that arise from errors associated with the regression and climate uncertainties that arise from differences between climate models (indicated in hatching).

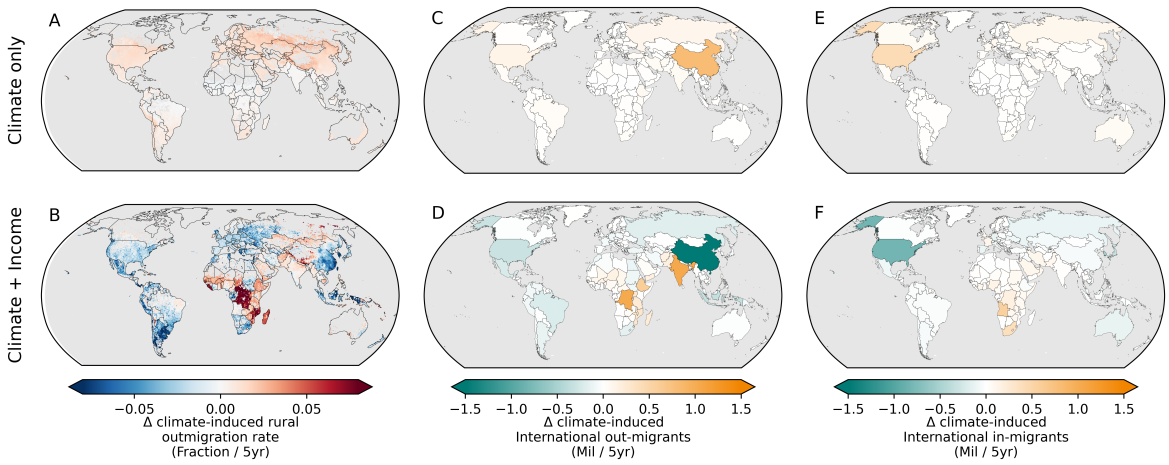

Figure 4: **Projections of climate-induced rural outmigration rates and international migration in 2050 relative to 2015.** Change in climate-induced rural outmigration rate (**A**, **B**), change in climate-induced international in-migrant number (**C**, **D**), and change in climate-induced international out-migrant number (**E**, **F**). The top row (**A**, **C**, **E**) shows results for projections in which income is fixed at 2015 levels and only the climate is changed. The bottom row (**B**, **D**, **F**) shows results for projections in which both income and climate change.

References and Notes

1. K. Schewel, S. Dickerson, B. Madson, G. Nagle Alverio, How well can we predict climate migration? A review of forecasting models. *Frontiers in Climate* **5**, 1189125 (2023), doi: 10.3389/FCLIM.2023.1189125/BIBTEX.

2. R. M. Beyer, J. Schewe, G. J. Abel, Modeling climate migration: dead ends and new avenues. *Frontiers in Climate* **5** (2023), doi:10.3389/FCLIM.2023.1212649/FULL.

3. A. De Sherbinin, *et al.*, Migration and risk: Net migration in marginal ecosystems and hazardous areas. *Environmental Research Letters* **7** (4) (2012), doi:10.1088/1748-9326/7/4/045602.

4. A. De Sherbinin, *et al.*, Global estimated net migration grids by decade: 1970–2000. *NASA Socioeconomic Data and Applications Center (SEDAC) at http://sedac. ciesin. columbia. edu/data/set/popdynamics-global-est-net-migration-grids-1970-2000* (2015).

5. A. Alessandrini, A. Deuster, C. Natale, Global estimates of net migration at high spatial resolution 1975-2020. *Publications Office of the European Union* (2023), doi:10.2760/06672.

6. S. Feng, A. B. Krueger, M. Oppenheimer, Linkages among climate change, crop yields and Mexico–US cross-border migration. *Proceedings of the National Academy of Sciences* **107** (32), 14257–14262 (2010), doi:10.1073/pnas.1002632107.

7. R. Cai, S. Feng, M. Oppenheimer, M. Pytlikova, Climate variability and international migration: The importance of the agricultural linkage. *Journal of Environmental Economics and Management* **79**, 135–151 (2016), publisher: Academic Press, doi:10.1016/J.JEEM.2016.06.005.

8. C. Cattaneo, G. Peri, The migration response to increasing temperatures. *Journal of Development Economics* **122**, 127–146 (2016), doi:10.1016/j.jdeveco.2016.05.004.

9. R. Hoffmann, A. Dimitrova, R. Muttarak, J. Crespo Cuaresma, J. Peisker, A meta-analysis of country-level studies on environmental change and migration. *Nature Climate Change* **10** (10), 904–912 (2020), doi:10.1038/S41558-020-0898-6.

10. IPCC, Climate Change 2022: Impacts, Adaptation and Vulnerability (2022), {https://www.ipcc.ch/report/ar6/wg2/downloads/report/IPCC_AR6_WGII_FinalDraft_FullReport.pdf}.

11. H. Benveniste, M. Oppenheimer, M. Fleurbaey, Climate change increases resource-constrained international immobility. *Nature Climate Change* **12** (7), 634–641 (2022), doi:10.1038/S41558-022-01401-W.

12. H. Benveniste, P. Huybers, J. Proctor, Global climate migration is a story of who and not just how many. *Nature Communications* **16** (1), 7752 (2025).

13. P. Bohra-Mishra, M. Oppenheimer, S. M. Hsiang, Nonlinear permanent migration response to climatic variations but minimal response to disasters. *Proceedings of the National Academy of Sciences of the United States of America* **111** (27), 9780–9785 (2014), publisher: National Academy of Sciences, doi:10.1073/PNAS.1317166111/-/DCSUPPLEMENTAL, https://www.pnas.org/content/111/27/9780https://www.pnas.org/content/111/27/9780.abstract.

14. A. Missirian, W. Schlenker, Asylum applications respond to temperature fluctuations. *Science* **358** (6370), 1610–1614 (2017), publisher: American Association for the Advancement of Science, doi:10.1126/SCIENCE.AAO0432/SUPPL_FILE/AAO0432_MISSIRIAN_SM.PDF, https://www.science.org/doi/abs/10.1126/science.aao0432.

15. G. Peri, A. Sasahara, The Impact of Global Warming on Rural-Urban Migrations: Evidence from Global Big Data. *National Bureau of Economic Research* (2019).

16. M. Beine, C. R. Parsons, Climatic Factors as Determinants of International Migration. *The Scandinavian Journal of Economics* **119** (2), 593–630 (2017), doi:10.1111/sjoe.12202.

17. V. Mueller, C. Gray, K. Kosec, Heat stress increases long-term human migration in rural Pakistan. *Nature Climate Change* **4** (3), 182–185 (2014), doi:10.1038/NCLIMATE2103.

18. C. Gray, V. Mueller, Drought and population mobility in rural Ethiopia. *World Development* **40** (1), 134–145 (2012), doi:10.1016/j.worlddev.2011.05.023.

19. C. Gray, V. Mueller, Natural disasters and population mobility in Bangladesh. *Proceedings of the National Academy of Sciences* **109** (16), 6000–6005 (2012), doi:10.1073/pnas.1115944109.

20. K. K. Rigaud, B. Jones, E. Bergmann, *et al.*, *Groundswell: Preparing for Internal Climate Migration*, Tech. rep., World Bank (2018), https://openknowledge.worldbank.org/handle/10986/29461.

21. M. Burzyński, C. Deuster, F. Docquier, J. De Melo, Climate Change, Inequality, and Human Migration. *Journal of the European Economic Association* **20** (3), 1145–1197 (2022), doi:10.1093/JEEA/JVAB054.

22. C. Cattaneo, *et al.*, Human migration in the era of climate change. *Review of Environmental Economics and Policy* **13**, 189–206 (2019), doi:10.1093/reep/rez008.

23. R. Hoffmann, G. Abel, M. Malpede, R. Muttarak, M. Percoco, Drought and aridity influence internal migration worldwide. *Nature Climate Change 2024 14:12* **14** (12), 1245–1253 (2024), doi:10.1038/s41558-024-02165-1, https://www.nature.com/articles/s41558-024-02165-1.

24. United Nations, *World Urbanization Prospects: The 2018 Revision* (United Nations) (2019), https://www.un-ilibrary.org/content/books/9789210043144.

25. J. V. Henderson, A. Storeygard, U. Deichmann, 50 Years of Urbanization in Africa : Examining the Role of Climate Change. *World Bank Policy Research Working Paper* (6925) (2014), publisher: World Bank, Washington, DC, doi:10.1596/1813-9450-6925, https://openknowledge.worldbank.org/handle/10986/18757.

26. A. I. Moreno-Monroy, M. Schiavina, P. Veneri, Metropolitan areas in the world. Delineation and population trends. *Journal of Urban Economics* **125**, 103242 (2021), doi:10.1016/J.JUE.2020.103242.

27. Y. Fan, H. van den Dool, A global monthly land surface air temperature analysis for 1948–present. *Journal of Geophysical Research: Atmospheres* **113** (2008), doi:10.1029/2007JD008470.

28. U. Schneider, A. Becker, P. Finger, E. Rustemeier, M. Ziese, GPCC Full Data Monthly Product Version 2020 at 0.5°: Monthly Land-Surface Precipitation from Rain-Gauges built on GTS-based and Historical Data (2020), doi:10.5676/DWD_GPCC/FD_M_V2020_050.

29. M. Kummu, M. Kosonen, S. Masoumzadeh Sayyar, Downscaled gridded global dataset for gross domestic product (GDP) per capita PPP over 1990–2022. *Scientific Data* **12** (1), 178 (2025).

30. V. Eyring, *et al.*, Overview of the Coupled Model Intercomparison Project Phase 6 (CMIP6) experimental design and organization. *Geoscientific Model Development* **9** (5), 1937–1958 (2016).

31. IPUMS, IPUMS International: Version 7.4 (2023), doi:10.18128/D020.V7.4, https://www.ipums.org/projects/ipums-international/d020.V7.4, dataset.

32. G. J. Abel, J. E. Cohen, Bilateral international migration flow estimates for 200 countries. *Scientific data* **6** (1), 82 (2019).

33. G. J. Abel, J. E. Cohen, Bilateral international migration flow estimates updated and refined by sex. *Scientific Data* **9** (1), 173 (2022).

34. M. Angelucci, Migration and Financial Constraints: Evidence from Mexico. *The Review of Economics and Statistics* **97** (1), 224–228 (2015), doi:10.1162/REST_a_00487, https://direct.mit.edu/rest/article/97/1/224/58218/Migration-and-Financial-Constraints-Evidence-from.

35. S. Bazzi, Wealth Heterogeneity and the Income Elasticity of Migration. *American Economic Journal: Applied Economics* **9** (2), 219–55 (2017), publisher: American Economic Association, doi:10.1257/APP.20150548.

36. P. Oliva, Migration and the environment: A look across perspectives. *Regional Science and Urban Economics* **107**, 104005 (2024), doi:10.1016/J.REGSCIURBECO.2024.104005, https://www.sciencedirect.com/science/article/pii/S0166046224000292.

37. M. Burke, S. M. Hsiang, E. Miguel, Global non-linear effect of temperature on economic production. *Nature* **527** (7577), 235–239 (2015).

38. T. Carleton, *et al.*, Valuing the global mortality consequences of climate change accounting for adaptation costs and benefits. *The Quarterly Journal of Economics* **137** (4), 2037–2105 (2022).

39. A. Alessandrini, D. Ghio, S. Migali, *Estimating net migration at high spatial resolution*, Tech. Rep. EUR 30261 EN, Publications Office of the European Union, Luxembourg (2020), doi:10.2760/383386, https://publications.jrc.ec.europa.eu/repository/handle/JRC121003.

40. M. Pesaresi, *et al.*, Advances on the Global Human Settlement Layer by joint assessment of Earth Observation and population survey data. *International Journal of Digital Earth* **17** (1), 2390454 (2024).

41. Global Human Settlements Layer (GHS), Functional Urban Areas (FUAs) 1km grid cells One-time urban area boundary representative of 2015 (2019), https://data.jrc.ec.europa.eu/dataset/347f0337-f2da-4592-87b3-e25975ec2c95, european Commission, Joint Research Centre (JRC).

42. W. Bank, World Development Indicators: GDP per capita (constant 2015 US$) (NY.GDP.PCAP.KD) (2025), https://data.worldbank.org/indicator/NY.GDP.PCAP.KD, accessed 2025-11-18; license CC BY 4.0.

43. J. Gao, Downscaling global spatial population projections from 1/8-degree to 1-km grid cells. *NCAR Technical Note NCAR/TN-537+STR* (2017), doi:10.5065/D60Z721H.

44. T. Wang, F. Sun, Global gridded GDP data set consistent with the shared socioeconomic pathways. *Scientific data* **9** (1), 221 (2022).

45. European Commission, Joint Research Centre (JRC), CIESIN, GHS-POP R2023A: Global Human Settlement Layer—Population Grid (1 km; 1975–2020) (2023), https://ghsl.jrc.ec.europa.eu/, gridded population counts derived from census and satellite data.

46. United Nations, Department of Economic and Social Affairs, Population Division, World Population Prospects 2022 (2022), https://population.un.org/wpp/, country-level births, deaths, and population totals.

47. GADM, GADM 4.1: Database of Global Administrative Areas (2023), https://gadm.org/, vector boundaries for ADM-0 and ADM-1 units.

48. W. Bank, World Bank Official Boundaries (2025), https://datacatalog.worldbank.org/search/dataset/0038272/world-bank-official-boundaries, high-resolution Admin 0/1/2, NDLSA, and ocean mask; shapefile, GeoPackage, and GeoJSON. Metadata last updated 2025-09-16.

49. G. J. Abel, Estimating global migration flow tables using place of birth data. *Demographic Research* **28**, 505–546 (2013).

50. R. Tibshirani, Regression shrinkage and selection via the lasso. *Journal of the Royal Statistical Society: Series B (Methodological)* **58** (1), 267–288 (1996).

51. A. Belloni, V. Chernozhukov, C. Hansen, Inference on treatment effects after selection among high-dimensional controls. *The Review of Economic Studies* **81** (2), 608–650 (2014).

52. M. C. Harding, C. Lamarche, Small steps with big data: using machine learning in energy and environmental economics. *Annual Review of Resource Economics* **13**, 469–488 (2021).

53. D. Hammami, T. S. Lee, T. B. Ouarda, J. Lee, Predictor selection for downscaling GCM data with LASSO. *Journal of Geophysical Research: Atmospheres* **117** (D17) (2012).

54. T. Vandal, E. Kodra, A. R. Ganguly, Intercomparison of machine learning methods for statistical downscaling: the case of daily and extreme precipitation. *Theoretical and Applied Climatology* **137** (1), 557–570 (2019).

55. F. Iglesias-Suarez, *et al.*, Causally-informed deep learning to improve climate models and projections. *Journal of Geophysical Research: Atmospheres* **129** (4), e2023JD039202 (2024).

56. A. Ahrens, C. B. Hansen, M. E. Schaffer, lassopack: Model selection and prediction with regularized regression in Stata. *The Stata Journal* **20** (1), 176–235 (2020).

57. V. Chernozhukov, C. Hansen, M. Spindler, Post-selection and post-regularization inference in linear models with many controls and instruments. *American Economic Review* **105** (5), 486–490 (2015).

Acknowledgments

The authors thank Marena Lin, Victoria Lawless, Ali Eshraghi, Ha Pham, Samuel Cohen, Alberto Fragoso and Keita Kadokura for helpful discussions and contributions to related research projects.

Funding: GK, JSW and KR were supported by the Carnegie Corporation through an Andrew Carnegie Fellowship. GK, JL, IG and KR were supported by the UC Institute on Global Conflict and Cooperation through a Security Implications of Climate Change grant. PP and KR acknowledge the Edward A. Frieman Endowed Presidential Chair in Climate Sustainability for providing funding for this research.

Author contributions: GK and KR conceived of the study and procured the funding. JSW conducted the climate data analysis. IG conducted the geospatial processing of population and migration data, constructed the main sample, and executed the data validation checks. PP executed the primary econometric analyses, Monte Carlo analysis and produced the projections. JL conducted the IPUMS analysis and developed the LASSO robustness tests. GK and KR supervised the research. All authors wrote the paper.

Competing interests: There are no competing interests to declare.

Data and materials availability: All data needed to evaluate the conclusions are in the paper, the Supplementary Materials, and publicly accessible repositories. Historical panel datasets comprise: net-migration 5-year grids (1980–2020) from the European Commission JRC (*5*); gridded population 5-year counts (1975–2020) (GHSL POP R2023a) (*40*); urban/rural boundaries defined by Functional Urban Areas from the Global Human Settlement Layer (*41*); and historical gridded income (GDP per capita) (*29*), temperature (*27*), and precipitation (*28*) data. For the in-

ternal–international migration linkage, we use IPUMS International microdata (Version 7.4 from 2024) (*31*) together with national income from the World Bank World Development Indicators (*42*).

Projection inputs are: gridded population (*43*) `[or replace with <POP-PROJ-DOI>]`, gridded GDP per capita (*44*) `[or replace with <INC-PROJ-DOI>]`, and climate projections from the CMIP6 Tier 1 ensemble (*30*). Bilateral international migration flow matrices used to allocate cross-border flows are available as a figshare collection (*32, 33*). Persistent identifiers (DOIs) and access URLs are provided here and/or in the References.

All code to replicate our main regressions, projections and figures can be found at https://github.com/ppolonik2/c

Supplementary materials

Materials and Methods

Supplementary Text

Figs. S1 to S3

Tables S1 to S4

References *(7-57)*

Supplementary Materials for
Income strongly moderates climate-driven migration

Gaurav Khanna[†], Pascal Polonik, Jessica Wan, Jacopo Lunghi, Ida Grigoryeva, Katharine Ricke[*†]

[*]Corresponding author. Email: kricke@ucsd.edu

[†]These authors contributed equally to this work.

This PDF file includes:

Materials and Methods

Data Sources and Processing

Population and net migration: We use the Global Human Settlement Layer (GHSL) gridded population counts at 1 km resolution in five-year intervals, derived from census sources and satellite-based settlement footprints (*45*). Net migration at 1 km resolution (1980–2020, five-year periods) is taken from the European Commission, Joint Research Centre (JRC) estimation framework (*39*), which applies the demographic balancing identity: cell-level population change equals natural increase (births minus deaths) plus net migration. Births and deaths are downscaled from UN DESA's World Population Prospects to the grid and allocated using a simple dasymetric approach (*39, 46*). We compute migration rates as (net migrants)/(population) at the cell level and exclude rural cells with implausible magnitudes (absolute rates > 1) to remove clear outliers.

The population and net migration data are derived from several observational units and imputations by the JRC research team to obtain the gridded population and net migration estimates:

1. **GHS-POP 2023 (gridded population)**

   The 2023 GHSL release utilizes built-up surface information from the GHS-BUILD-S product with census-based population totals from CIESIN/GPWv4.11 and UN DESA country-level population series (*45, 46*). Built-up comes from satellite imagery aggregated to the following "anchor epochs": 1975, 1990, 2000, and 2014 (Landsat) and 2018 (Sentinel-2 at 10 m). Each build-up area observation is based on higher-frequency satellite imagery, aggregated across years to allow for sufficient corrections for cloud cover and other missing data observations. The product also includes a residential versus non-residential (RES vs. NRES) classification at 10 m and mean building height at 100 m. Between anchor years, the built-up fields are spatio-temporally interpolated or extrapolated to produce a 5-year time series from 1975 to 2020 at 100 m resolution. Population totals are taken from official census datasets and the UN DESA 2022 time series at the (sub)national region level (subnational data on admin level 1 and 2 are used where available from national census data for the overlapping years). GHSL then interpolates the national/subregional population totals to grid cells within each region, using the built-up area and building heights distribution as weights. Regarding the question of temporal independence, not every time step is an independent satellite observa-

tion. Built-up area is directly observed at the anchor epochs and is modeled in between, while population is not a direct satellite measurement at any epoch. Instead, subregion-level census estimates are allocated to grid cells using the built-up surface as the spatial distribution prior. In the 2023 release, the last observed population benchmark is 2020, which is the last year of data we include in historically observed population estimates. For instance, for the 2020 snapshot, the gridded population uses 2020 census and UN DESA region totals and the 2018 built-up epoch to allocate people across space (*45, 46*).

2. **JRC Grid-Cell Net Migration Imputations**

   The net-migration grids at 1 km resolution in five-year periods from 1980 to 2020 combine GHSL population grids at the start and end of each five-year window with births and deaths from UN DESA World Population Prospects (WPP) (*5, 46*). For each cell and 5-year interval, net migration equals population change minus natural increase, where natural increase is births minus deaths. Because births and deaths are not observed at the cell level, they are downscaled and allocated to the cell regions based on the population and built-up surface as weights. This is an indirect residual method in which population change is fixed by the GHSL grids, births and deaths come from UN WPP together with their spatial allocation, and the residual is net migrants. The JRC applies country-specific validation/consistency checks, such as reconciling census estimates with cell-to-subregion re-aggregation, and validates against UN DESA and Eurostat aggregates. The implications are that the migration series inherits the GHSL and UN WPP measurement structure, GHSL population provides the spatial baselines, UN WPP provides vital statistics, with prior net-migration values not feeding later ones (*39, 46*).

   One of the key novelties is that these net migration estimates explicitly account for different fertility/mortality across the urban-rural continuum of geographic areas (cities, towns, and rural areas). Where UN Demographic Yearbooks (DYB) provide area-specific rates, those are used; where not, area-specific rates are imputed from the country level using regressions and constraints that ensure the mix of area rates reproduces the WPP country total. “Towns” are treated as the arithmetic mean of city and rural rates when direct data are missing.

   Area types follow the Degree of Urbanization (DoU) three-way split: (1) cities, (2) towns

& (3) rural. DYB/WPP typically provide **two** groups (urban, rural). JRC maps birth/death stats for urban areas to DoU cities and rural rates to DoU rural areas, and defines the **towns** rate as the simple arithmetic mean of the city and rural rates for the same country–period. Where DYB area-specific series are missing or discontinuous, city/rural rates are imputed at the country level (e.g., via auxiliary regressions and borrowing from demographically similar neighbors), and the resulting triplet {city, town, rural} is constrained so that the population-share-weighted average of area-type rates reproduces the WPP national natural change for that period. Each cell is assigned a DoU class using the $t + 5$ classification for the interval $t \rightarrow t + 5$ (so that the area-type reflects end-of-period settlement status), and cell-level natural change is computed by multiplying the area-type rate by the cell's five-year average population and duration.

Net migration at the cell level is then obtained as a **residual**:

$$Net\ Migration_{c,t,t+5} = \left(Pop_{c,t+5} - Pop_{c,t}\right) - Natural\ Change_{c,t,t+5}$$

where c indexes a grid cell (at the working resolution for the migration grids), t is the start year of the quinquennium; $t+5$ is the end year, $Pop_{c,t}$ and $Pop_{c,t+5}$ are the GHSL population counts for cell c at the start and end of the five-year window, $Net\ Migration_{c,t,t+5}$ is net migration in cell c over the interval t to $t + 5$, $Natural\ Change_{c,t,t+5}$ is births minus deaths in cell c accumulated over t to $t + 5$.

By construction, aggregating cells matches UN WPP national totals for population, natural change, and the implied national net migration residual. The imputation of vital rates is conducted **at the country level by area-type** (cities/towns/rural); there is no ADM-1 or ADM-2 modeling of fertility/mortality in the published method, although cells inherit geographic heterogeneity through their population paths and DoU classifications. JRC applies country-specific checks (e.g., reconciling census vintages and geometry changes, rescaling GHSL to WPP national totals) and validates against UN DESA and Eurostat aggregates and selected sub-national series. Importantly, each quinquennium is **recomputed independently** from GHSL $t, t + 5$ populations and period-specific area-type vital rates; prior net-migration grids do not feed later ones (*39, 46*).

Urban/Rural Boundaries: Urban areas are identified using the GHSL Functional Urban Areas (FUA) boundaries representative of urban agglomeration areas in 2015, which delineate contiguous urban agglomerations using population, density, and commuting criteria at 1 km resolution (roughly 30') (*41*). We overlay the working 5-arcmin grid on FUA polygons and drop any 5-arcmin cell entirely within a FUA. Cells that partially intersect a FUA are treated as *border* cells: we compare the 30' urban pixels (roughly 1km) to the GHSL population grid and retain only the portion outside the FUA when constructing the rural sample. We use the FUA urban boundaries as fixed, with no changes over time, thus providing a single consistent rural-cell analysis sample, both for the historically observed trends and future projections. Figure S1 illustrates an example of a large urban area (the City of São Paolo and the surrounding region, and a zoomed-in sample of the City of São Paolo, respectively) and how it fits to the differently-sized grids.

While ideally, we would want to process all gridded population and migration spatial data at its finest 1km resolution, assigning each grid cell as urban or rural to leverage the file resolution of the urban area boundaries as well, this proved to be infeasible with our computing power for the entire globe. As a reasonable medium, we are analyzing some of the border cells at the 5-arcmin level prior to aggregating to the level of climate cells at half-degree. As a result, we process the population and migration 5-year rasters in several aggregation steps described below, motivated by sample region exploration and feasibility tests (also illustrated in Figure S1). The detailed processing algorithm is described below.

Below, we describe the step-by-step process of rural-only sample creation, focusing on removing areas over cities in the initial sample calculation. Note that we aimed for minimal spatial processing in QGIS, prioritizing full code-based replication in Stata and Python code outside of QGIS. This contributes to the analysis choices made below. The sample creation steps are as follows:

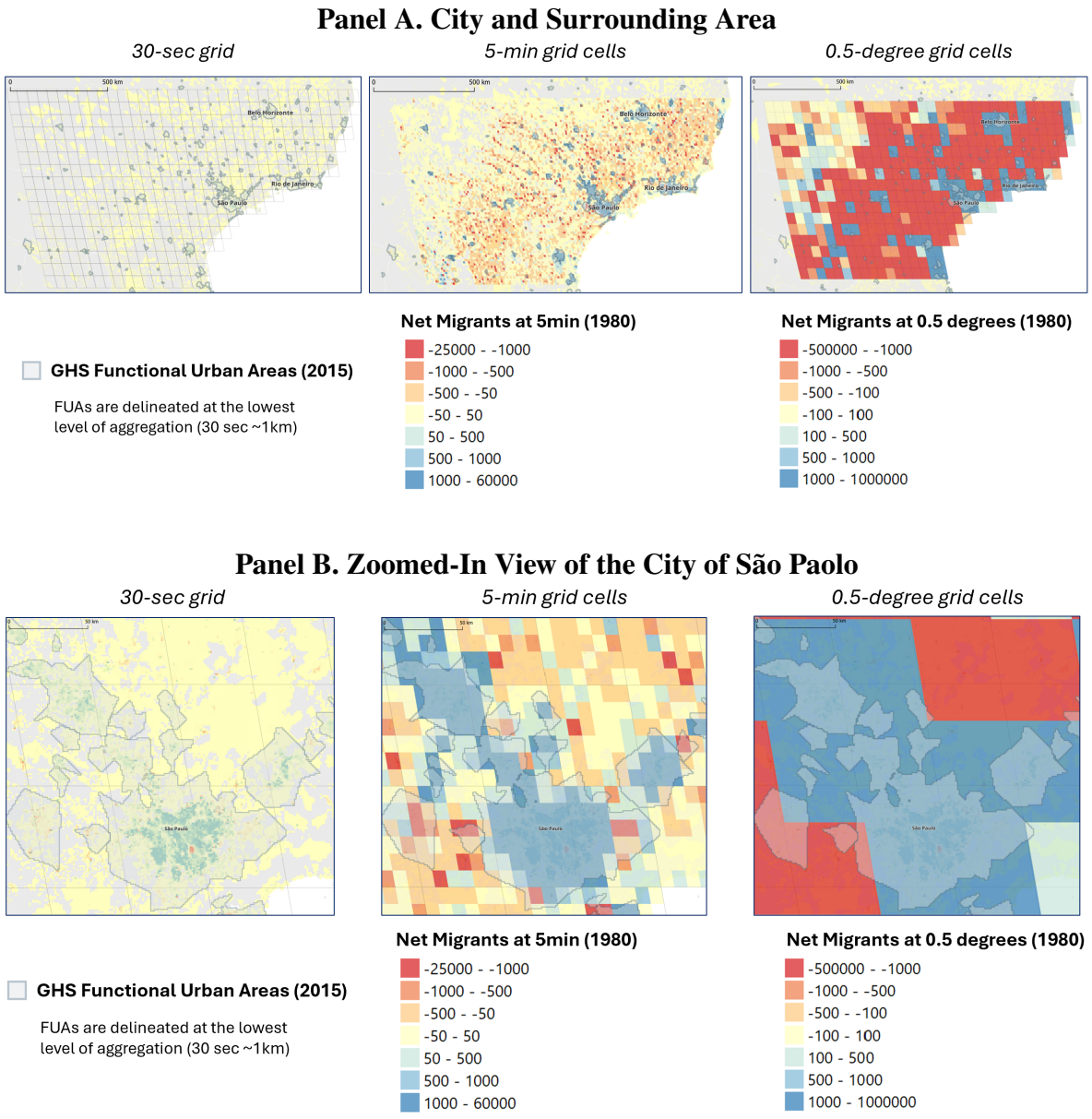

Figure S1: Sample Region in Latin America (City of São Paolo and Surrounding Region) with Urban Area Boundaries and Net Migration Estimates. Left: 30-arc-second grid with GHSL Functional Urban Areas (FUAs; 2015, gray) (*41*). Center: 5-arc-minute cells colored by net migrants in 1980 (*5*). Right: 0.5° (half-degree) analysis units colored by net migrants in 1980 (*5*). In both panels, red tones denote net out-migration and blue tones denote net in-migration. Note that a half-degree cell is substantially bigger than the urban area and its components, motivating the intermediate analysis and rural sample construction at the 5-arc-minute level.

1. **Aggregate to a workable resolution**: Aggregate the finest resolution of the underlying data to match the climate data grid: 1km (vectorized as points for one year) and 30 sec (raster) to 5-arcmin grid cells

2. **Reduce the extent of to relevant land cells**: Create the relevant 5-arcmin grid based on the climate data grid extent, including the following:

    - Keep only cells over land
    - Remove Antarctica, resulting in 2.3 million 5-arcmin grid cells (*36 for 30 sec count)
    - Take the cells with non-missing population data

3. **Construct the rural cell sample**: Remove 5-arcmin grid cells corresponding to urban areas (overlapping with urban area polygons), resulting in two types of overlap:

    - Identify cells overlapping with FUA to drop later
      $\Longrightarrow$ drop each 5-arcmin cell that is within the urban area polygon from the rural sample
    - Partial overlap with FUA
      $\Longrightarrow$ each 5-arcmin cell partially overlapping with the urban area polygon is designated as an urban "**border cell**" to conduct additional processing to isolate net-migration estimates corresponding to the rural areas immediately surrounding the urban polygon
      $\Longrightarrow$ separate out 30sec raw observations that are outside the urban polygon within 5-arcmin border cells (computationally feasible given a smaller number of border cells)

4. **Construct the final rural-only sample** by removing areas corresponding to urban areas using a new approach (See an example of the sample regions in Figure S2)

    - Take all complete rural cells (those not overlapping with FUAs at all)
    - Add the rural sections of border cells

Panel A. Complete Rural Cells and Rural Sections of Border Cells with Net Migration (1980)

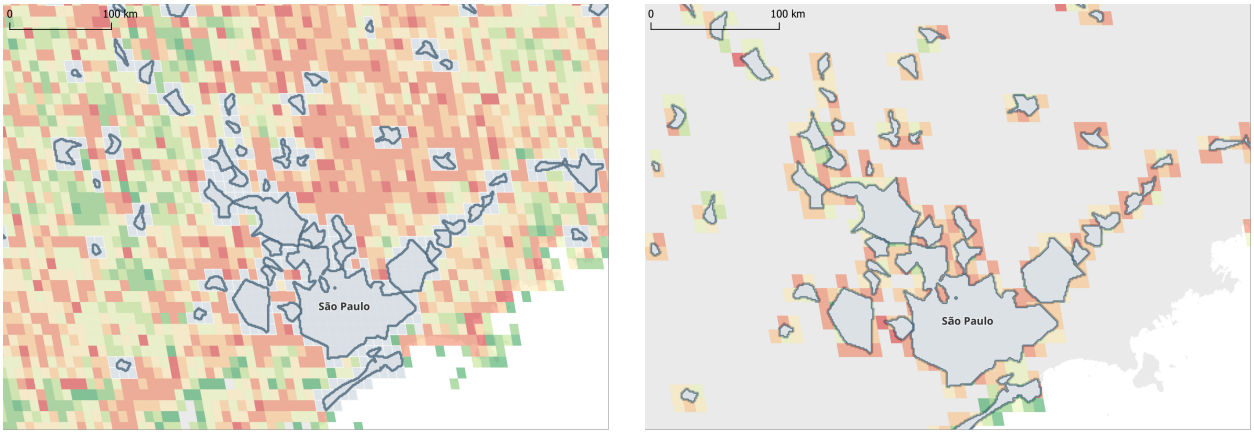

Panel B. Border Cells near the City of São Paolo with Rural Population Share per Cell (1975)

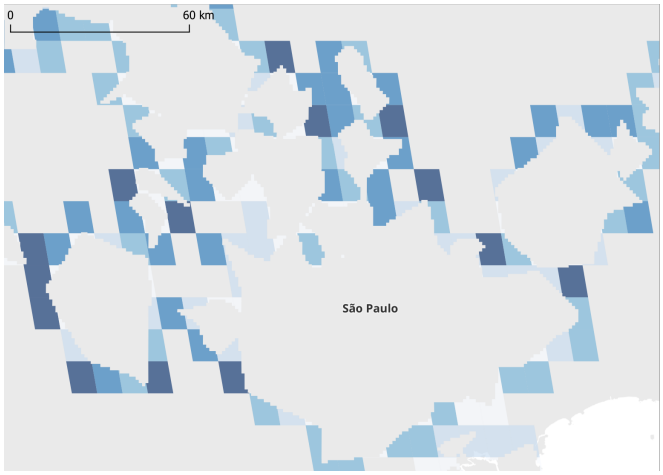

Figure S2: Rural Sample Construction at 5-Arc-Minute Level (City of São Paulo and Surrounding Area Sample Region) with Urban Area Boundaries, Rural Cells with Net Migration Counts, and Rural Population Share. Top-left: 5-arcmin cells fully outside of urban boundaries ("complete rural cells") colored by net migrant counts in 1980 (*5*). Top-right: 5-arcmin border cell sections outside the city boundary, with rural portions retained after masking the net migration and population layers by GHSL Functional Urban Areas (FUAs; 2015, gray) (*41*); colors again show 1980 net-migration counts. Bottom figure: border cells shaded by the share of each 5-arc-minute cell's population that lies *outside* the FUA in 1975 relative to total population of the entire 5-arcmin cell. In the net-migration maps, red denotes negative (net out-migration) and green denotes positive (net in-migration). In the rural-share map, deeper blue indicates a larger rural population share (0–1). FUAs are treated as fixed boundaries; cells fully inside a FUA are excluded from the rural sample, and intersecting cells contribute only their non-FUA portion.

Matching Climate Grid to Administrative-Unit Identifiers: All demographic inputs are aggregated from 30-sec/1 km to a 5-arcmin grid (land only; Antarctica excluded). The final data preparation step for the main analysis involves matching each grid cell to its administrative region identifier since migration patterns vary by national and subnational borders. We intersect each 0.5° cell with subnational administrative regions one level below national (ADM-1). Specifically, we:

1. Construct the wider global set of national and subnational identifiers combining the subnational admin-1 polygon layers from GADM v4.1 (*47*) and the World Bank subnational shapefiles (*48*)[1]

2. Assign each 5-arcmin cell its ADM1 code (or ADM0 where ADM1 is not available) via a spatial join

3. Map each cell to the 0.5°×0.5° global tile to each overlapping administrative region

4. Sum population and net migrants over all 5-arcmin cells within each (tile, ADM1) unit for each 5-year period

This spatial aggregation results in an observational panel of cell–year units at the *half-degree* × *ADM1* level, preserving within-country heterogeneity, which include population and net migration (count and rates) in each cell and a rural/urban cell designation for each half-degree cell (0.5°).

Income (GDP per capita)

1. **Historical Series of Gridded GPD per Capita**: Historical gridded per-capita gross domestic product (GDP) data was taken from a novel dataset matching our historical analysis time-period (*29*). The dataset interpolates economic activity over space in a manner similar to the GHSL population using a mix of administrative and satellite-imagery-derived data, providing an input for the imputed spatial distribution of economic activity at the 1km grid cell level.

   Kummu et al. (2025) (*29*) build an annual, fine-resolution GDP per capita (PPP, 2017 international USD) series for 1990–2022 by harmonizing national and subnational sources

[1]We use both sources since they have complementary sets of subnational region polygons, with the combination of the two providing a larger set of subnational admin1 units.

and then downscaling them to administrative level 2 before gridding. First, they assemble national GDP per capita time series and fill missing years with linear interpolation and a documented extrapolation routine. Next, they collect subnational (admin 1) GDP per capita from OECD, Eurostat, and national statistical offices, convert these to ratios relative to the national average, and interpolate the ratio time series; at the ends of series, the last observed ratio is carried forward/backward. They then downscale the admin 1 to admin 2 ratio with a machine-learning model (boosted ensemble trees) trained on independent predictors aggregated to admin 1: a gridded urbanization level derived by combining GHSL population with UN World Urbanization Prospects to match each country's annual urban share, travel time to the nearest city over 50,000 in population, the national Gini coefficient, and national GDP per capita. Predicted admin 2 ratios are multiplied by the harmonized national series to obtain absolute admin 2 GDP per capita; values are provided both as polygons and on a 5-arc-minute grid. Finally, total GDP is computed by multiplying GDP per capita by GHSL population, and the product is calibrated to preserve national totals and is provided with annual data at the 1km grid cell level. Reported performance is high (cross-validation $R^2 = 0.79$, test sample $R^2 = 0.80$; Pearson $R = 0.88$ with observed subnational data) (*29*).

2. **Historical Gridded GDP Processing:** For each 5' land cell, we extract the annual series and spatially align it to our working 5' grid. Cells are joined to first-level administrative boundaries and half-degree tiles, where each duplicate coordinate cell for different admin units is collapsed to a single cell. The GDP data (*29*) relies on the same population grid input as our net migration data (*45*), which we use to get at GDP per capita estimates.

   We use these to (i) construct a cell-year total GDP series (by multiplying GDP per capita by GHSL population) and (ii) compute cell-year GDP per capita using the same GHSL population counts used elsewhere in the paper. We then aggregate GDP and population to the analysis unit (half-degree × ADM-1) and compute per-capita GDP at that scale; rural/urban subsets follow our FUA-based filter. This pipeline preserves the annual frequency, harmonizes geography with the migration sample, and keeps income denominators consistent across outcomes.

Throughout the paper, we refer to $GDP_{per\ cap}$ interchangeably as income, as it is a proxy for local income/wealth generation. This dataset is generated at 5-arcmin spatial resolution, which we then aggregate to 0.5-degree resolution using the rural-cell selection and then scaling up to a larger spatial unit as described above for the population and net migration data. The final 0.5-degree cell total GDP is then divided by the 0.5-degree cell population in each corresponding year.

3. **GPD per capita projections:** Projected gridded SSP $GDP_{per\ cap}$ data was taken from (*44*), and we use population data from (*43*). Both datasets have 1 km spatial resolution, which we aggregate to 5 arcmin before performing the same rural aggregation to 0.5-degree resolution as for the datasets above. The population data are required for the aggregation since we only use the $GDP_{per\ cap}$ associated with rural grid cells. To avoid discontinuities between the historical and SSP $GDP_{per\ cap}$ datasets, we only use the growth rate from the SSP data, and add it to the historical data.

Final Sample Restrictions: Once we aggregate all population and migration data with appropriate urban-rural identifiers, we obtain an initial sample of approximately 76,000 land half-degree ($0.5^\circ \times 0.5^\circ$) grid cells with some population data. We then drop all half-degree cells that contain fewer than 50 underlying 1 km $\times$ 1 km cells with non-missing population data (about 7,000 cells), then drop cells with no migration data (about 3,600 cells) and cells with GDP per capita below 100 (about 100 cells). After these restrictions, the baseline half-degree sample consists of 64,600 unique grid-cell–administrative-unit combinations, of which 8,300 are urban cells. In constructing the analysis variables, roughly 1,000 cells have missing values in at least one of the key variables (population or migration). We winsorize GDP per capita at an upper bound of $200,000 and winsorize extreme migration rates at +2 and -1 for each 5-year period. For the years 1980–2015, about 30–50 cells per year are top-coded at +2 and about 75–220 cells per year are bottom-coded at -1, whereas for 2020 alone, 180 cells would be top-coded at +2 and 60 cells would be bottom-coded at -1. Because the distribution of migration rates in 2020 exhibits a markedly different pattern of outliers, with many more top-coded observations, we exclude 2020 from our main analysis. Our resulting rural sample contains approximately 56,300 unique rural grid cells, of which about 55,000 have non-missing migration data.

Temperature and Precipitation Data:

1. **Historical observational datasets:** Gridded historical monthly 2-meter air temperature data are obtained from the Global Historical Climatology Network version 2 and the Climate Anomaly Monitoring System (GHCN-CAMS) (*27*), and precipitation data are from the Global Precipitation Climatology Centre (GPCC) V2020 (*28*). We subset the temperature and precipitation data from 1950 to 2019 to develop historical relationships with migration patterns. Both temperature and precipitation data products are based on a network of thousands of station observations that are interpolated to have continuous temporal and spatial coverage at 0.5-degree horizontal resolution.

2. **Projected climate model output:** Projected gridded monthly temperature and precipitation data are obtained from the Coupled Model Intercomparison Project Phase 6 (CMIP6) Tier 1 experiments (*30*), which encompasses a range of potential future climate scenarios under the Shared Socioeconomic Pathways (SSP1-2.6, SSP2-4.5, SSP3-7.0, and SSP5-8.5). We note that the number of models used in this analysis varies between 25 and 30 models, depending on scenario, due to data quality issues (SSP1-2.6: 28, SSP2-4.5: 29, SSP3-7.0: 25, and SSP5-8.5: 30). Each model is regridded to 0.5-degrees to match the historical climate data resolution for analysis. Historical CMIP6 climate data is used between 1960 and 2019, and SSP CMIP6 data is used between 2020 and 2060. All CMIP6 temperature and precipitation data are bias corrected using the monthly climatological mean historical temperature and precipitation datasets, respectively, averaged between 1990 and 2019.

3. **Construction of Metrics:** As our analysis aims to quantify the relative importance of climate and climate change on migratory flows, we characterize climatic conditions by computing three distinct sets of temperature and precipitation variables, reported in Fig. S5. First, we compute 5-year averages of temperature and precipitation to align with the frequency of the migration dataset used in this study. This is our standard measure of the baseline climate state and most commonly used in the climate econometric literature to date.

   Next, we develop two specialized metrics to capture different temporal scales of climate change that could influence migration patterns. We compute a trend metric to characterize the rate of change in typical conditions (Fig. S5). Monthly trends are computed as a least-squares,

piecewise linear regression where the trend for the 5-year period of interest (blue) is anchored to the terminal point of the trend line of the preceding 30-year baseline period trend (red). As such, the trend metric captures the extent to which typical conditions in precipitation and temperature evolve over time. Finally, we calculate a variability metric as the mean absolute residual (original data minus least-squares estimate) of the 5-year period of interest divided by the mean absolute residual of the baseline period minus one (Fig. S5). By normalizing the ratio, positive values of the variability metric indicate an increase in variability over time, while negative values identify an increase in the predictability of climate conditions. These calculations are conducted on the same datasets for the past and future as described in the previous section.

Internal and International Migration: As individuals move within a country, we expect part of the climate-induced migratory flows to occur across national borders. To project country-level cross-border net migration, we proceed in two steps.

First, we gather data on internal and international migration from two sources. We use the Integrated Public Use Microdata Series-International (IPUMS-International) dataset, a collection of census microdata, to derive the relationship between internal and international migration at the country level (*31*). From individual-level records, we collect information on whether respondents migrated within their country of residence or abroad. An individual of age 5+ is considered migrated if they have changed residence since a reference point 5 years ago (*migrate5*). Both migrating within and outside a major administrative unit without crossing national borders is considered internal migration. Only migration outside the country of residence is considered international. We then aggregate these data to construct internal (mig) and international (MIG) migration rates. We use Natural Earth shapefiles for administrative aggregation. The IPUMS dataset provides information for 43 countries between 1985 and 2017. Our final sample contains 90 observations. After aggregation, we obtain a cross-sectional dataset of country-year observations, which we use to examine the correlation between internal and international migration by estimating the following regression:

$$\mathrm{MIG}_{it} = \alpha + \beta\, \mathrm{mig}_{it} + \epsilon_{it} \tag{S1}$$

where the outcome variable is the international out-migration flow from country i and year t, and

the main independent variable is the internal migration rate in the same country and period. The parameter $\hat{\beta}$ captures the relationship between the two flows.

Table S1: **IPUMS data is available for 43 countries between 1985 and 2017**. We use IPUMS-International individual data to compute country-year observations on internal and international migration flows, combined into a cross-sectional dataset. The table reports the combinations of countries and years available.

Country	Years	Country	Years	Country	Years	Country	Years
ARG	1991,2001	DOM	2002,2010	ISR	1995,2008	PHL	2000,2010
BOL	1992,2001,2012	ECU	1990,2001,2010	ITA	2011	PRT	1991,2001,2011
BRA	1991,2000,2010	ESP	1991	MAR	2004	PRY	1992,2002
BWA	2011	FJI	1986,1996,2007	MEX	1990,1995,2000,2005,2010	SEN	1988,2002,2013
CAN	1991,2001	FRA	2006	MNG	2000	SLE	2015
CHE	1990,2000	GHA	2000	MOZ	1997,2007	TTO	2000
CHL	2002	GRC	1991,2001	MUS	1990,2000,2011	URY	1985,1996,2006,2011
CHN	1990,2000	GTM	1994,2002	MYS	1991,2000	USA	1990,2000
CMR	2005	HND	1988,2001	NIC	1995,2005	VNM	1989,1999,2009
COL	1985,1993,2005	HTI	2003	NPL	2001,2011	ZAF	2001
CRI	2000,2011	IDN	1985,1990,1995,2000,2005,2010	PER	2007		

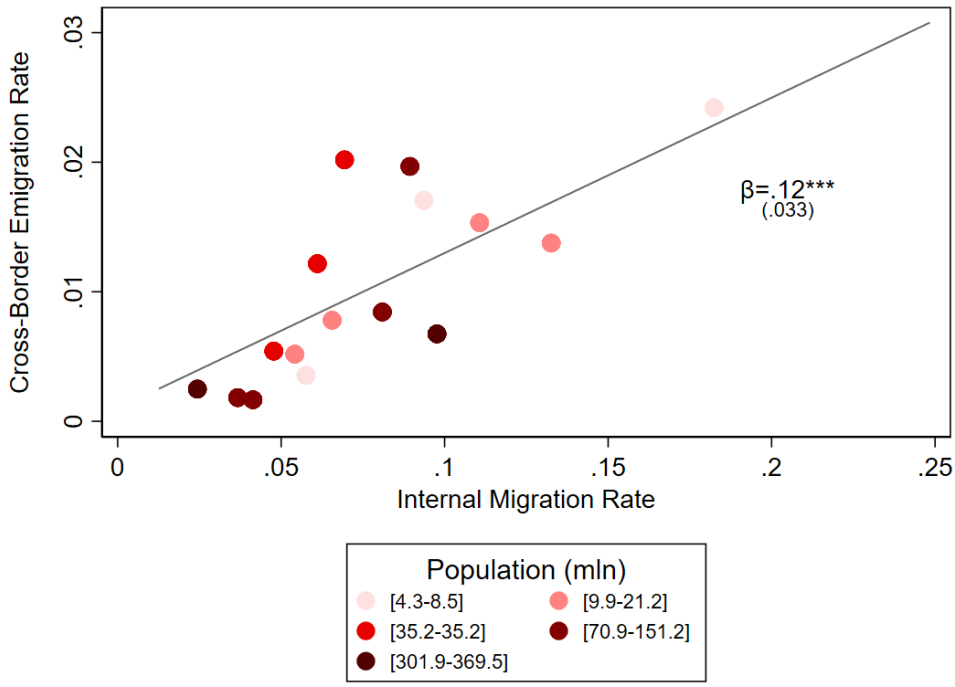

Figure S3: **Positive relationship between internal and international migration.** We use a cross-sectional dataset of country-year observations on internal and international migration flows to estimate the relationship between the two, as specified in Equation S1. A 1% increase in internal migration rates is associated with a 0.12% increase in cross-border migration. Countries are grouped into 16 bins based on population. *** p<0.01, ** p<0.05, * p<0.1.

Second, we then gather bilateral international migration flows between all pairs of 200 countries for five five-year periods from mid-year (July 1) 1990 to mid-year (June 30) 2015 from (*33*). We use the data to construct a matrix of global bilateral international migration flows. In our baseline analysis, we use migration corridors between countries calculated using demographic accounting, pseudo-Bayesian average of migrant transitions and stayers, according to a closed accounting system. Demographic accounting methods estimate bilateral migration flows by transforming stock data into flow estimates while adjusting for natural population changes (*49*). Refer to (*33*) for detailed information on alternative methods for computing migration flows. An example of bilateral migratory flows is given in Figure S4.

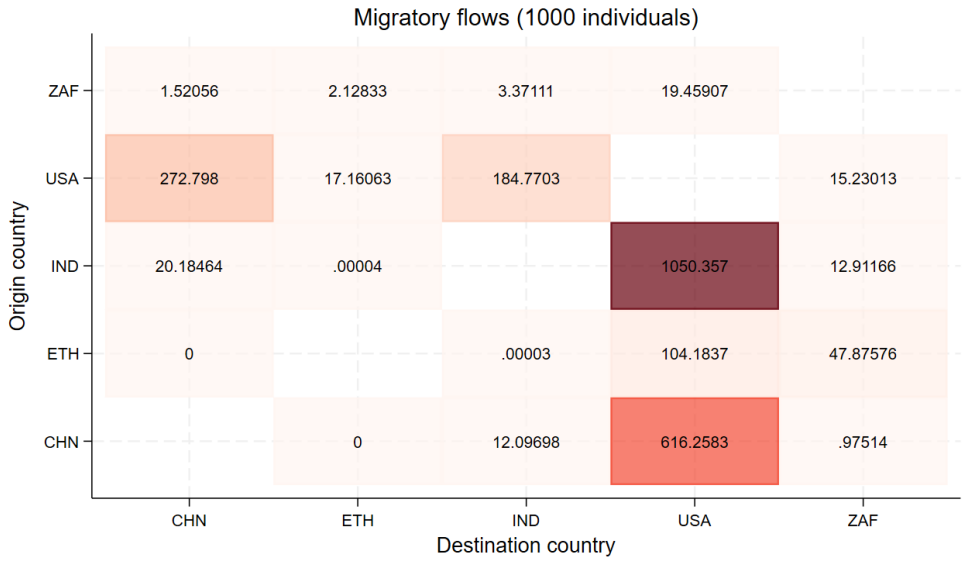

Figure S4: **Bilateral international migration flow estimates from (*33*).** The authors provide estimates of international migratory corridors in 2010, obtained via demographic accounting, through a pseudo-Bayesian average of migrant transitions and stayers.

We combine the data with the projected levels of internal migration to derive net migration levels in country j, according to the following:

$$\begin{aligned}\Delta \text{MIG}_{it} &= -\,\text{mig}_{it} \cdot \hat{\beta} + \sum_j \text{mig}_{jt} \cdot \hat{\beta} \cdot \frac{\text{MIG}_{ij}}{\sum_j \text{MIG}_j} \\ &= \hat{\beta} \left[\sum_j \text{mig}_{jt} \cdot \frac{\text{MIG}_{ij}}{\sum_j \text{MIG}_j} - \text{mig}_{it} \right]\end{aligned} \tag{S2}$$

where $\text{mig}_{it} \cdot \hat{\beta}$ is the calculated outflow of international migrants leaving country i. The same stock in country j ($\text{mig}_{jt} \cdot \hat{\beta}$) constitutes an international inflow of migrants to country i, weighted by the existing bilateral migration relationships as per (*33*). The weight is computed using the ratio between the inflow of migrants to country i from country j (MIG_{ij}), and the total outflow of migrants from country j to all destinations ($\sum_j \text{MIG}_j$).

Historical Relationship Between Climate and Migration

Regression analysis. Our preferred specification is

$$\text{mig}_{it} = \sum_{r=1} \sum_{k=1} \phi_{rk} \cdot \text{CLIM}_{it}^{r} \cdot \text{INCOME}_{i}^{k\top} + \mu_i + \theta_t + \varepsilon_{it} \tag{S3}$$

where mig_{it} represents the net outmigration rate for grid cell i at time t. $\text{CLIM}_{it}^{r} = \left(T_{it}, T_{it}^2, P_{it}\right)$ is vector of r climate measures including temperature (T), temperature squared $\left(T^2\right)$ and precipitation levels (P). The vector $\text{INCOME}_{i}^{k} = \left(1, \log(GDP)_i, (\log(\text{GDP}))_i^2\right)$ contains instead k regressors, the log-transformed income in cell i and its square. The measure of cell GDP is time-invariant, and is obtained from historical gridded per capita gross domestic product (details provided in the Data Sources and Processing section). Income terms that are not interacted are effectively captured by the fixed effects, which includes cell (μ_i) and year (θ_t) level fixed effects. We remove the upper and lower 0.1% of T, Ttrend, and P values from the analysis to avoid outliers. This removes about 0.2% of the global population from the analysis. We cluster standard errors by administrative unit 1 (e.g., states), and additionally cluster by country as a sensitivity test. We also test versions of this equation without the quadratic income interactions and without any income interactions.

Selection of regressors (LASSO): It is uncertain whether individual migration choices are more sensitive to baseline climate conditions or their evolution over time. On the one hand, if migratory responses to climate are triggered under broadly similar conditions across regions, absolute levels of temperature and precipitation may serve as the best predictors of climate-induced migration. On the other hand, if households adapt their lifestyle to local baseline climatic conditions, then it may be deviations from the status quo—rather than the levels themselves—that prompt migration. Controlling for both climate variability and changing trends can help clarify these dynamics. Yet including multiple climate metrics in a single specification greatly increases dimensionality, with numerous potential interaction terms and fixed effects. The resulting collinearity risks adding noise and biasing projections of climate-related migration. To address this, we first assess the relevance of these regressors using a machine learning (ML) approach for variable selection before expanding the specification.

ML techniques allow flexibility and statistical discipline in selecting a regression model with many potential regressors, minimizing researcher bias and arbitrary exclusion under an unclear prior on effect heterogeneity. We employ the LASSO ("least absolute shrinkage and selection operator") shooting algorithm (*50*) under a rigorous penalization approach (*51*). The LASSO is a popular

machine learning tool in economic and environmental research (*52*), particularly useful for the selection of predictions in climate modeling applications (*53–55*). Moreover, as we are interested in inference on the effect of regressors in our fixed effects model rather than simple prediction, the LASSO produces post-estimation coefficients that are easier to interpret due to the linear structure of the problem, making it more suitable for variable selection than tree models in our framework (e.g., random forest).

We start with the following specification model:

$$\text{mig}_{it} = \sum_{r=1}\sum_{k=1}\beta_{rk} \cdot \text{CLIMCHANGE}_{it}^{r} \cdot \text{INCOME}_{i}^{k\top} + \mu_i + \theta_t + \varepsilon_{it} \tag{S4}$$

where the net outmigration rate measure for cell i at time t (mig_{it}) is regressed on an extended vector of r climate terms, $\text{CLIMCHANGE}_{it}^{r} = \left(1, T_{it}, T_{it}^2, T\text{var}_{it}, T\text{var}_{it}^2, T\text{trend}_{it}, P_{it}, P\text{var}_{it}, P\text{var}_{it}^2, P\text{trend}_{it}\right)$, as well as cell ($\mu_i$) and time ($\theta_t$) fixed effects. The LASSO algorithm minimizes the mean squared error subject to a penalty on the absolute size of coefficient estimates for each predictor. Let the generic regression model, where the time index is omitted without loss of generality, be:

$$y_i = \mathbf{X}_i'\beta + e_i \tag{S5}$$

where β represents a vector of regressors. To establish the number of predictors to be included in the model, the algorithm estimates the following:

$$\hat{\beta}(\lambda) = \arg\min \frac{1}{n}\sum_{i=1}^{n}\left(y_i - \mathbf{X}_i'\beta\right)^2 + \frac{\lambda}{n}\sum_{r}\sum_{k}\nu_{r,k}|\beta_{rk}| \tag{S6}$$

where, given a sample of n observations, λ is the parameter regulating the overall penalty level, while $\nu_{r,k}$ is a predictor-specific complementary penalty loading for a variable k within group r. To provide penalty parameter values to the model, we apply the "rigorous" approach to penalization, executed through the Stata package `rlasso`. Rigorous LASSO application provides penalization parameters by achieving an optimal rate of convergence for prediction and parameter estimation (*56*). In this sense, rigorous application offers a setup to account for the large number of controls and fixed effects in our model while assuming our variable of interest (climate dynamics) to be exogenous conditional on observables (*51, 57*).

Table S2: **Regression results from the estimation of the migration and climate relationship with augmented climate terms using LASSO**. The regression includes cell and year fixed effects. Standard errors are clustered at the cell level. Primary variables are partialled out from the calculation of regressor-specific penalties, and as a result are always present in the model. Selected covariates indicate regressors surviving the penalization from the LASSO algorithm. Included covariates that enter the model but are discarded by the algorithm are also reported.

Variable	β(LASSO)	β(OLS)
Primary variables		
P	-0.0489	-0.0502
		(0.0063)
$P \times \log(\text{GDP})$	0.0118	0.0121
		(0.0015)
$P \times (\log(\text{GDP}))^2$	-0.0007	-0.0007
		(8.8E-5)
T	0.0131	0.0172
		(0.0081)
$T \times \log(\text{GDP})$	0.0026	0.0014
		(0.0019)
$T \times (\log(\text{GDP}))^2$	-0.0003	-0.0003
		(0.0001)
T^2	8.5E-5	-8.9E-5
		(0.0003)
$T^2 \times \log(\text{GDP})$	-0.0002	-0.0001
		(7.6E-5)
$T^2 \times (\log(\text{GDP}))^2$	1.6E-5	1.3E-5
		(4.6E-6)
Selected covariates		
T trend	0.0027	0.0048
		(0.0005)
T var $\times (\log(\text{GDP}))^2$	1.3E-5	7.9E-5
		(1.5E-5)
Included covariates		
P ; $P \times (\log(\text{GDP}))^2$; $P \times \log(\text{GDP})$; P trend ; P trend $\times$ $(\log(\text{GDP}))^2$; P trend $\times \log(\text{GDP})$; P var ; P var $\times (\log(\text{GDP}))^2$; P var $\times \log(\text{GDP})$; P var^2 ; P var$^2 \times (\log(\text{GDP}))^2$; P var^2 $\times \log(\text{GDP})$; T ; $T \times (\log(\text{GDP}))^2$; $T \times \log(\text{GDP})$; T trend ; T trend $\times (\log(\text{GDP}))^2$; T trend $\times \log(\text{GDP})$; T var ; T var $\times$ $(\log(\text{GDP}))^2$; T var $\times \log(\text{GDP})$; T var^2 ; T var$^2 \times (\log(\text{GDP}))^2$; T var$^2 \times \log(\text{GDP})$; T^2 ; $T^2 \times (\log(\text{GDP}))^2$; $T^2 \times \log(\text{GDP})$		

We fit Equation S4 using the rigorous LASSO algorithm. We partial out all regressors included in our baseline specification (*primary variables*), as well as year and cell fixed effects, so that the algorithm will not suppress these measures. This, in turn, allows us to understand whether alternative climate measures could still help explain a substantial part of the residual variation in the regression. The results are reported in Table S2.

In addition to the regressors already included in the model, the LASSO selects only 2 of the 18 supplementary climate metrics, suggesting that the baseline climate variables already possess substantial explanatory power. The selected terms point to a potential role of temperature variability and evolving trends. The effect of temperature trends is relatively straightforward, as they appear to influence migration in a manner analogous to temperature levels. By contrast, the interaction between temperature variance and the squared log of income is less readily interpretable.

It is important to emphasize that the LASSO imposes no prior structure on the nature of the regressors and, as such, provides no inherent rationale for the inclusion of interaction or higher-order terms. We interpret these results as evidence that the category of climate metrics—specifically temperature trends and variance—may influence historical climate migration rates. We therefore include them, along with the respective income interactions, in some of our supplemental specifications as extensions and robustness checks. However, their influence on projections is small, and they are therefore not included in our preferred specification (Fig. S11).

Projections

We estimate future migration rates by taking the difference between projected migration rates for 2050 and subtracting modeled migration rates for 2015. We do this both for fixed and time-varying income

Internal Migration Varying Income: In the time-varying income case, we use $GDP_{per\ cap}$ from (*44*) and climate model output for the climate variables. $GDP_{per\ cap}$ is bias corrected to match our historical data, as described in the Data Sources and Processing section above. For our main projection, we use the average from all available climate models, though we also estimate climate uncertainty from individual climate models, as described in the Monte Carlo and Uncertainty section below. Importantly, we do not include the $GDP_{per\ cap}$ and $GDP^2_{per\ cap}$ terms in the projections,

as they are controls and do not constitute climate migration.

Internal Migration Fixed Income: In the fixed-income case, we do not allow $GDP_{per\ cap}$ to change over time and instead fix it at 2015 levels. The treatment of climate and controls is the same as in the time-varying income case described above. We include this projection to demonstrate the impact of climate alone.

Cross-border Migration: To project cross-border migration, we multiply the projected grid-cell level migration rate by the grid-cell population, and multiply this total number of migrants in a country by the international fraction (a constant of 0.12 described in the "Internal and International Migration" section). We then apportion these international migrants to countries based on the matrix of between-country flows from (*33*). Lastly, we sum the number of migrants by the destination country. This process is identical for the fixed-income and varying-income projections, except that the initial migration rates are taken from the fixed or varying income projections, respectively.

Climate uncertainty and statistical uncertainty: Future climate is available from many different climate models (see Temperature and Precipitation data section). Our main analysis uses the model mean as the input, while we use each of the models individually to quantify the climate uncertainty.

To quantify the statistical uncertainty in the projections, we take a Monte-Carlo approach. We re-run the main estimating equation using only a subset of the panel dataset. In one case, we randomly sample a pre-specified fraction of the dataset (e.g., only use half the sample) and repeat this 100 times. This gives us a set of 100 estimates of the coefficients; each set is used for its own projections, which yields a range. Lastly, as a sensitivity test, we also sample by administrative unit 1 (e.g., states), rather than randomly sampling the whole dataset. In other words, we generate a set of estimated coefficients using only one random grid cell from each admin 1 unit, and repeat that test 100 times.

Supplementary Text

Robustness Overview

To test the robustness of the main selected model specification we:

1. Run linear regressions at the grid cell level to test whether local linear estimates match the global nonlinear estimate;

2. Demonstrate the role of the income interactions by building the equation, one interaction at a time and show the results for two clustering units for standard errors (admin unit 1, and country);

3. Show the distribution of coefficients from a conservative Monte Carlo analysis, and

4. Show projection results for specification variations.

Local-linear: We run a linear regression between migration rate and temperature at each rural grid cell to check whether the 95% confidence interval of the resulting estimates contains the marginal effect of the global estimate, evaluated at that grid cell, in tests similar to (*37*). We test this regression with linear and quadratic income controls, and with a precipitation control; these slight variations make very little difference to the result. The cumulative density of cells that pass the test indicates that about 78% of grid cells pass the test using the 95% confidence interval (Fig. S8). The grid cells are dispersed throughout the globe and do not clearly occur in any particular region, with at least 72% of cells in each continent passing the test (Fig. S9).

Build interactions: We show results with a variety of specifications that build up to our preferred specification (Table S3), with only climate terms and fixed effects (i.e., no income interactions). Only the precipitation term shows any statistical significance. In other words, the temperature terms alone do not have a statistically significant relationship with rural outmigration rates. Adding linear income interactions increases statistical significance, but still does not yield a precise result. Only when including both quadratic temperature with quadratic income interactions do the results become highly significant (all terms $p<0.01$). Including a quadratic precipitation term eliminates all statistical significance of the precipitation terms, which we interpret as overfitting; we therefore limit our preferred specification to the more parsimonious linear term. The projections are not substantially impacted by these decisions (Fig. S11, compare 1 to 0). The above results qualitatively hold when using country clustering of standard errors instead of admin 1 clustering of standard errors (Table S5). As expected, the p-values are substantially higher when clustering by country, but almost all terms still have $p<0.1$ (the T^2 term is the exception, with $p=0.103$).

Uncertainty Analysis: We next conduct a Monte Carlo analysis in which we sample a subset from our input panel dataset, and re-estimate the coefficients. We resample 85% of grid cells, 50% of grid cells, and one grid cell per admin 1 unit (Fig S10). Each is repeated 100 times to generate a distribution of coefficients. As expected, sparser sampling results in wider distributions of coefficients. However, even for the extremely conservative admin 1 sampling, the sign of all of the coefficients is robust. The average magnitude is also consistent, with the magnitudes tending slightly larger for the conservative admin 1 sampling.

Alternative Specifications: Lastly, to justify our preferred specification, we show that our results are consistent when using alternative specifications with more terms (Fig S11). As in the main text, we show results for both fixed and time-varying income. We test whether including quadratic precipitation, or interactions between temperature and precipitation, substantially influence the outcome and find that they do not. We then add trend and variability metrics (see Methods section on Construction of Metrics and LASSO). We include temperature and precipitation trend and variability terms and find that - especially when including time-varying income projections - the results are stable. We then also test the impact of replacing the quadratic temperature term with an interaction between temperature and mean temperature. The fact that this variant also does not substantially change the projections indicates that the global interpretation of the quadratic temperature term - that results from the retention of some cross-sectional variation in quadratic fixed-effect regressions - is robust.

Next, we include a specification in which we adopt a more conservative definition of the urban-rural division. We take as rural only the half-degree grid cells that do not contain any urban grid cells (i.e., drop any cells that were split into urban and rural at the 5 arc minute resolution).

Lastly, we include lagged climate terms. Though there is some expected variation in the results, none of these variants yield substantively different results.

We also run our analysis for only urban locations instead of rural ones (Table S6). Results using admin 1 unit clustering of standard error indicate that effects are statistically significant at $p<0.05$ for temperature, but not for precipitation. When clustering by country, two of nine climate terms just meet the $p<0.1$ threshold, while the rest do not.

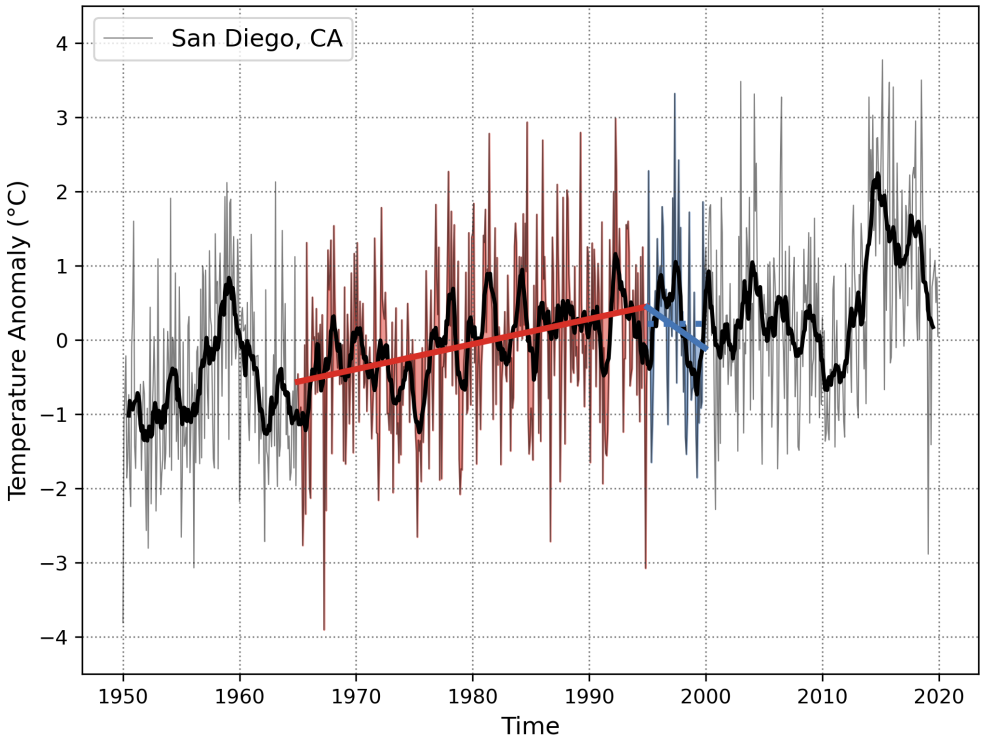

Figure S5: **Schematic of climate metric construction for historical temperature in San Diego, California.** Time series of temperature anomalies in San Diego, California (33.5° N, 117° W) illustrating example climate metrics for the period 1995-2000. The metrics are 5-year mean temperature level (blue dotted line), trend (solid red and blue piecewise lines), and variability (shaded red and blue area).

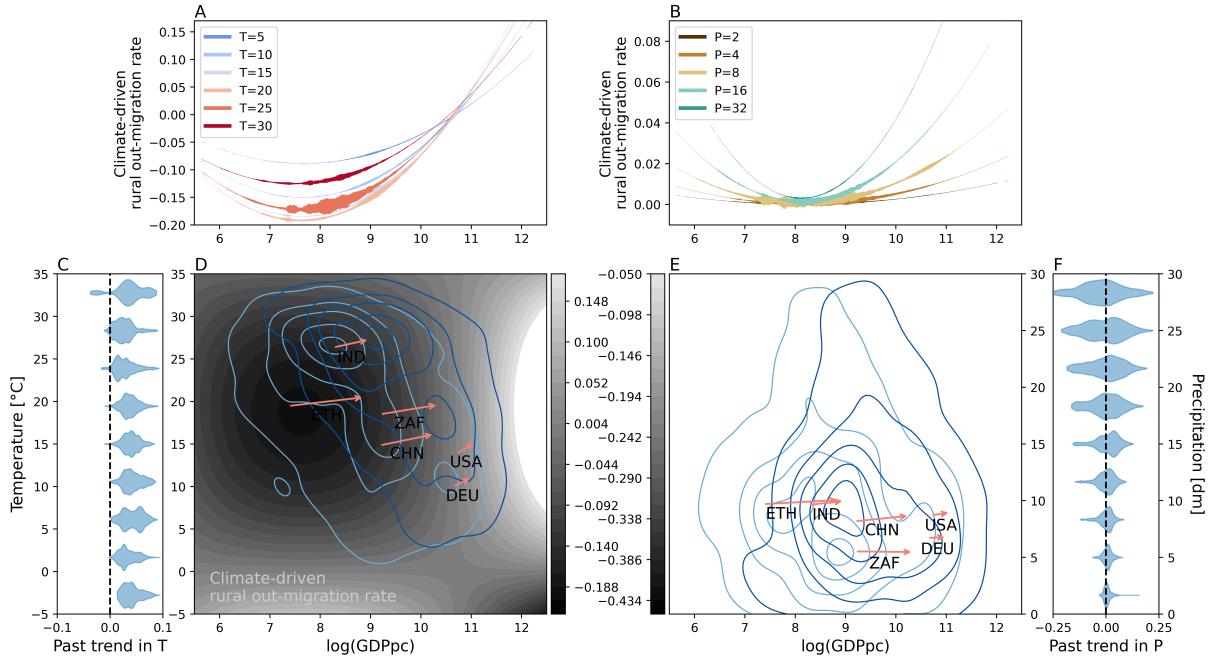

Figure S6: **Climate-driven migration rate using only urban grid cells.** Same as Fig. 2, except using urban grid cells instead of rural grid cells.

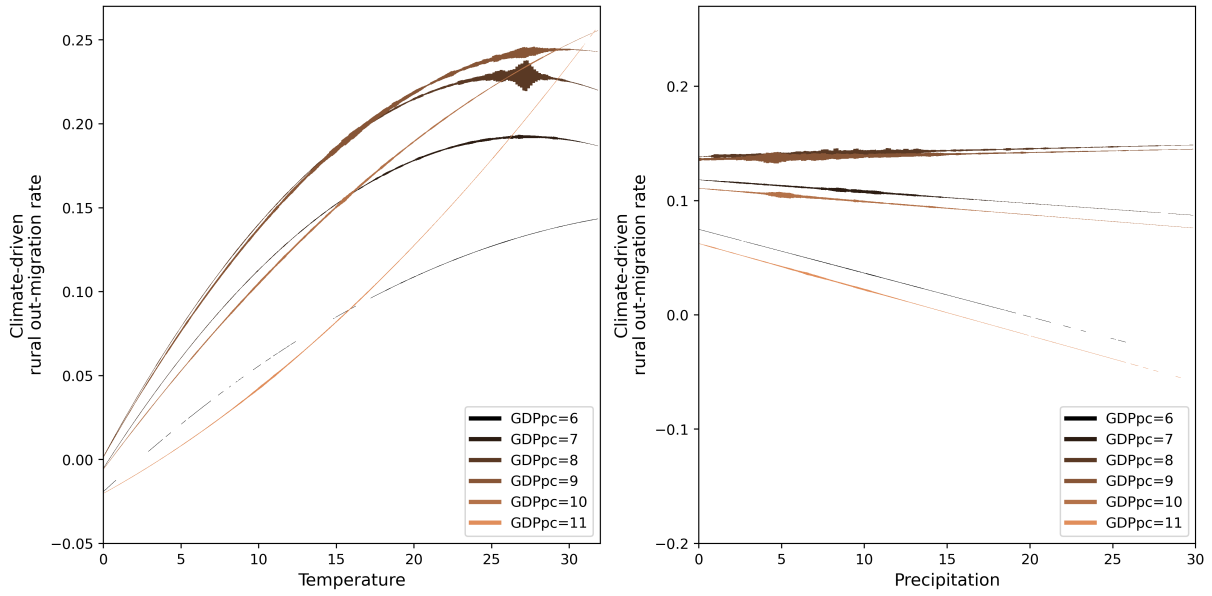

Figure S7: **Climate-driven rural outmigration rate as a function of temperature and precipitation.** Colors indicate different $logGDP_{per\ cap}$ levels. Results are based on the preferred specification. Line width is proportional to the number of observations in each temperature and precipitation bin. This is an alternative visualization of the same results shown in Figure 2.

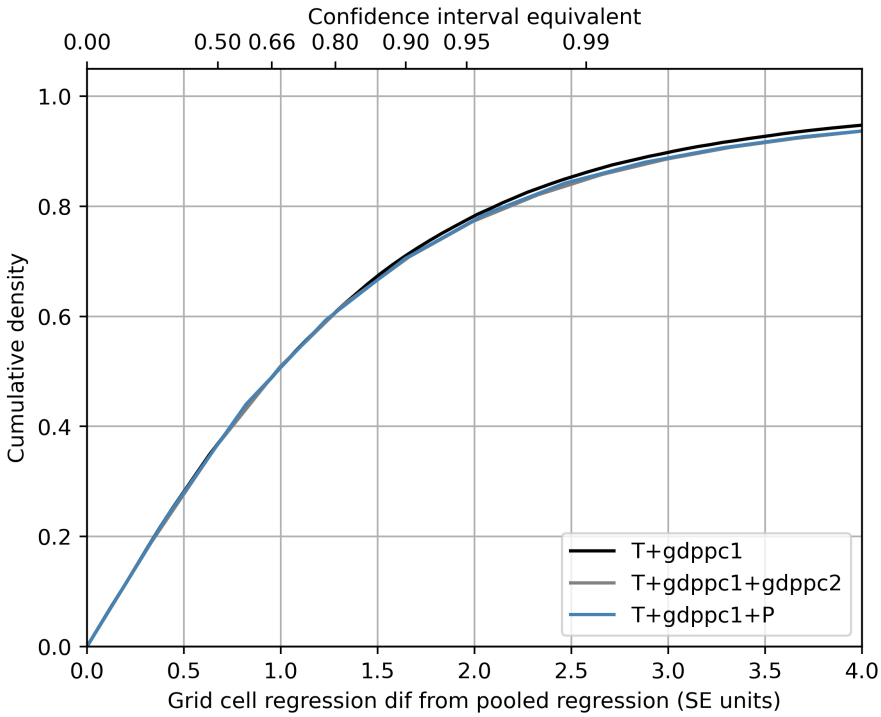

Figure S8: **Cumulative density of passed local-linear robustness checks** We conduct a linear robustness check on each grid cell and then check whether the slope of the global regression - evaluated at the grid cell mean values - lies within the confidence interval of the local regression. The chosen confidence interval will determine whether a grid cell passes the check. This chosen confidence is indicated on the top x-axis, with the corresponding standard error shown on the lower x-axis. This figure is population-weighted. The three lines are for slightly different specifications of local-linear regressions and yield essentially identical results.

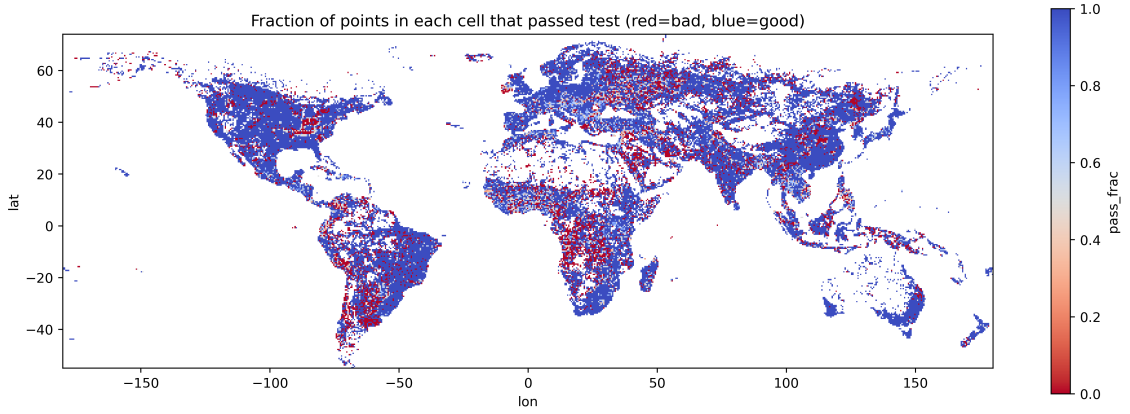

Figure S9: **Map indicating which grid cells pass the local-linear test at the 95% confidence interval.** This map corresponds to the same results shown in Figure S8. Since the unit of analysis is split grid cells, we have aggregated back to the grid cell level using population-weighting and show the population fraction that passed the local-linear test in the color bar.

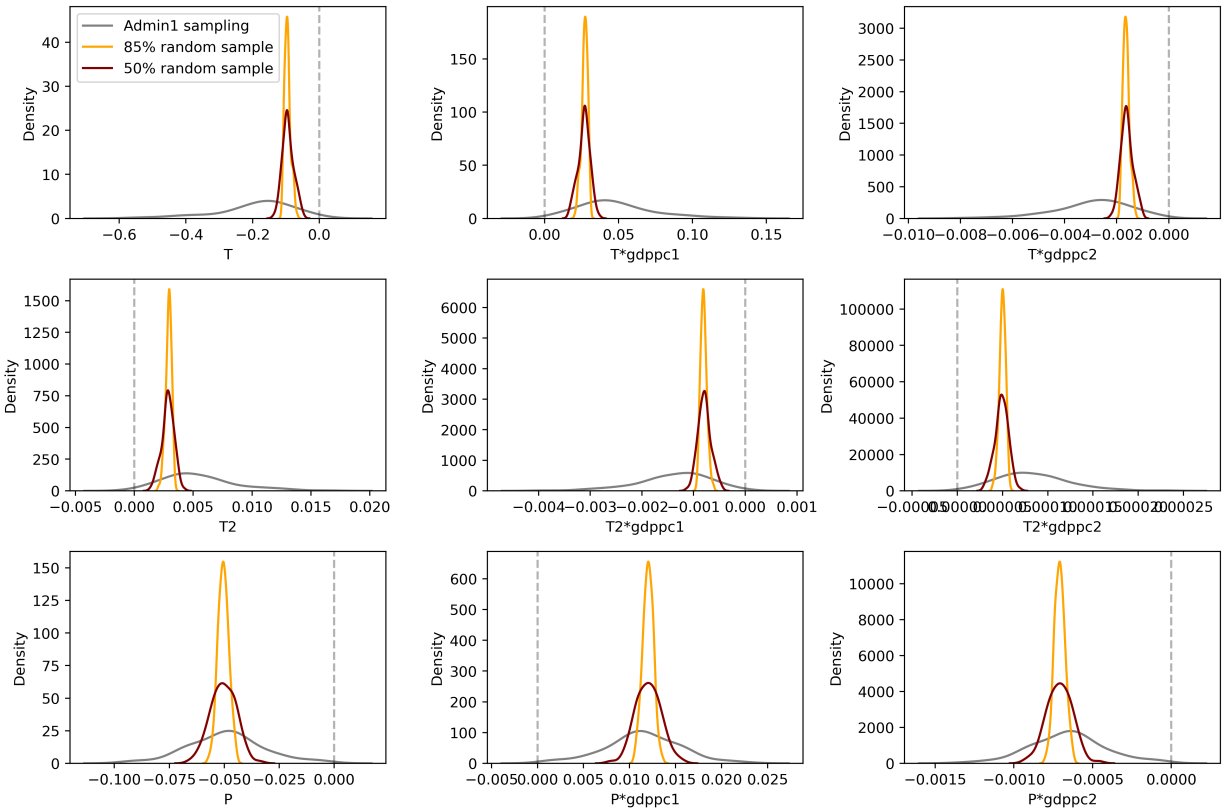

Figure S10: **Distributions of coefficients from the Monte Carlo analysis** Each panel shows a different coefficient, each distribution shows the result of 100 panel regressions that result from re-sampling the dataset using the method indicated in color. The dashed vertical line is the zero reference line.

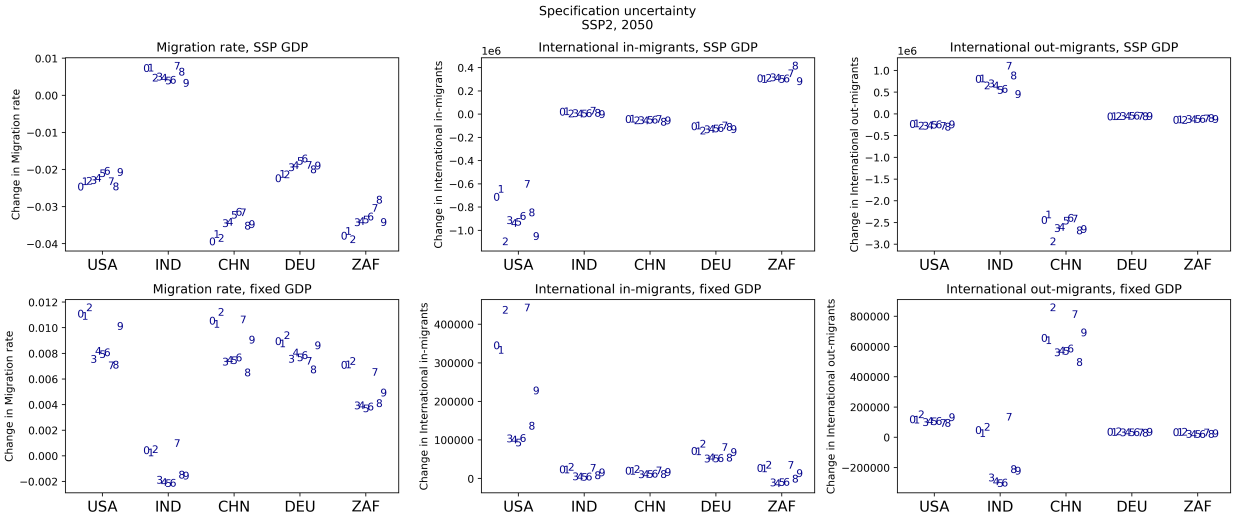

Figure S11: **Projected change in migration rate (left), international in-migrants (middle) and international out-migrants (right) in 2050 under SSP2 for a select group of large countries, for several different model specifications**. The top row contains projections using time-varying income, and the bottom row corresponds to projections using fixed income. Each number corresponds to a specification, listed here. Unless otherwise specified, every listed term is also included with linear and quadratic income interactions. 0: preferred specification for reference. 1: Same as 0, but with additional P^2 terms. 2: Same as 1, but with additional $T * P$ terms. 3: Same as 1, but with additional Ttrend terms. 4: Same as 3, but with additional Ttrend and Tvar terms. 5: Same as 4, but with additional Ptrend terms. 6: Same as 5, but with additional Pvar terms. 7: Same as 0, the T^2 terms are replaced with Tmean*T terms. 8: Same as 1, except excluding entries that contain any urban entries within their half-degree grid cells. 9: The same as 1, but including a lag-1 T, T^2, and P terms (as with all other listed specifications, all interacted with linear and quadratic income).

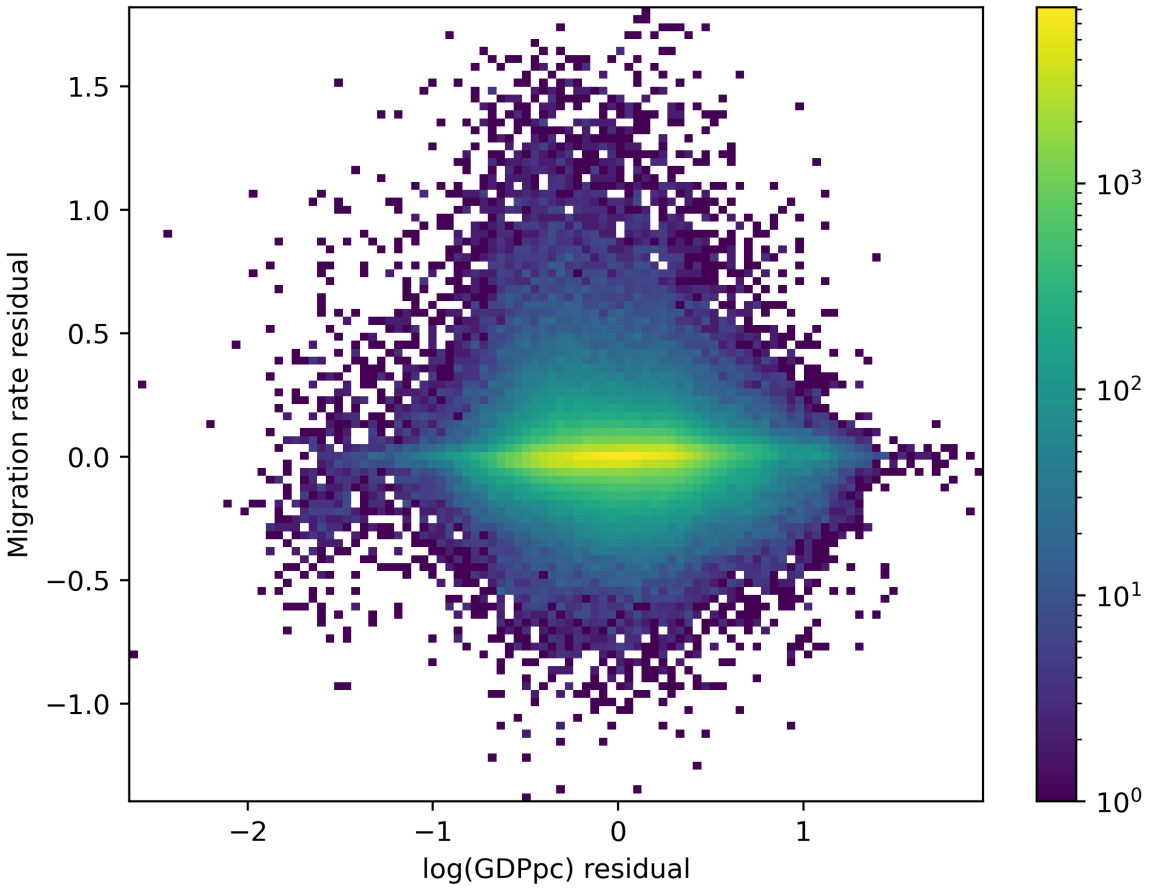

Figure S12: **2D histogram of residualized log(GDPpc) and rural outmigration rate.** Colors represent the number of points in each bin on a log scale. Both variables are residualized individually by removing just space and time fixed effects. The R^2 is 0.003.

Table S3: **Regression results to justify the chosen specification.** Standard errors are clustered by admin 1 units (e.g., states). Each regression has unit and time fixed effects. We do not find statistical significance unless we use quadratic temperature with quadratic $GDP_{per\ cap}$ interactions. Including P^2 does not add additional information and reduces statistical significance.

	Dep var: Net Migration rate				
	(1)	(2)	(3)	(4)	(5)
	Climate-Only	Income Quadratic	Quad + Income	Full Interactions	Full Interactions + P^2
T	0.002	0.002	0.014**	-0.096***	-0.101***
	(0.004)	(0.013)	(0.006)	(0.034)	(0.034)
T × Ln GDP pc		0.001	-2.34E-04	0.027***	0.029***
		(0.003)	(0.001)	(0.008)	(0.008)
T × Ln GDP pc^2		-1.23E-05		-0.002***	-0.002***
		(1.92E-04)		(0.001)	(0.001)
T^2	2.91E-05		-4.65E-04**	0.003***	0.003***
	(7.75E-05)		(1.84E-04)	(0.001)	(0.001)
T^2 × Ln GDP pc			3.21E-05*	-0.001***	-0.001***
			(1.84E-05)	(2.62E-04)	(2.63E-04)
T^2 × Ln GDP pc^2				5.01E-05***	5.21E-05***
				(1.58E-05)	(1.59E-05)
P	-0.001**	-0.053***	-0.003	-0.050***	-0.033
	(4.24E-04)	(0.016)	(0.002)	(0.015)	(0.027)
P × Ln GDP pc		0.013***	2.37E-04	0.012***	0.008
		(0.004)	(2.48E-04)	(0.004)	(0.006)
P × Ln GDP pc^2		-0.001***		-0.001***	-4.45E-04
		(2.18E-04)		(2.10E-04)	(3.91E-04)
P^2					-0.001
					(0.001)
P^2 × Ln GDP pc					1.64E-04
					(2.33E-04)
P^2 × Ln GDP pc^2					-9.76E-06
					(1.40E-05)
Ln GDP pc		-0.038	-0.027***	-0.209***	-0.198***
		(0.050)	(0.005)	(0.066)	(0.069)
Ln GDP pc^2		0.001		0.011***	0.010**
		(0.003)		(0.004)	(0.004)
Constant	-0.024	0.190	0.103*	0.828***	0.784***
	(0.045)	(0.201)	(0.061)	(0.274)	(0.286)
Cell FE	✓	✓	✓	✓	✓
Year FE	✓	✓	✓	✓	✓
Mean dep var	-0.02	-0.02	-0.02	-0.02	-0.02
SD dep var	0.19	0.19	0.19	0.19	0.19
N	381,052	378,529	378,529	378,529	378,529
R^2 (inclusive)	0.63	0.64	0.64	0.65	0.65
R^2 (within)	0.00	0.03	0.02	0.03	0.03

Notes: Outcome is the outmigration rate. T = temperature, P = precipitation. All specifications include cell and year fixed effects. Standard errors in parentheses. Significance: $^{***}p < 0.01$, $^{**}p < 0.05$, $^{*}p < 0.10$.

Table S4: **Regression results to justify the chosen specification.** Standard errors are clustered by admin 1 units (e.g., states). Each regression has unit and time fixed effects. We do not find statistical significance unless we use quadratic temperature with quadratic $GDP_{per\ cap}$ interactions. Including P^2 does not add additional information and reduces statistical significance.

	Dep var: Net Migration rate					
	(1)	(2)	(3)	(4)	(5)	(6)
	Income-only	Climate-Only	Income Quadratic	Quad + Income	Full Interactions	Full Interactions + P^2
T		0.002	0.002	0.014**	-0.096***	-0.101***
		(0.004)	(0.013)	(0.006)	(0.034)	(0.034)
T × Ln GDP pc			0.001	-2.34E-04	0.027***	0.029***
			(0.003)	(0.001)	(0.008)	(0.008)
T × Ln GDP pc^2			-1.23E-05		-0.002***	-0.002***
			(1.92E-04)		(0.001)	(0.001)
T^2		2.91E-05		-4.65E-04**	0.003***	0.003***
		(7.75E-05)		(1.84E-04)	(0.001)	(0.001)
T^2 × Ln GDP pc				3.21E-05*	-0.001***	-0.001***
				(1.84E-05)	(2.62E-04)	(2.63E-04)
T^2 × Ln GDP pc^2					5.01E-05***	5.21E-05***
					(1.58E-05)	(1.59E-05)
P		-0.001**	-0.053***	-0.003	-0.050***	-0.033
		(4.24E-04)	(0.016)	(0.002)	(0.015)	(0.027)
P × Ln GDP pc			0.013***	2.37E-04	0.012***	0.008
			(0.004)	(2.48E-04)	(0.004)	(0.006)
P × Ln GDP pc^2			-0.001***		-0.001***	-4.45E-04
			(2.18E-04)		(2.10E-04)	(3.91E-04)
P^2						-0.001
						(0.001)
P^2 × Ln GDP pc					1.64E-04	
						(2.33E-04)
P^2 × Ln GDP pc^2						-9.76E-06
						(1.40E-05)
Ln GDP pc	0.0910***		-0.038	-0.027***	-0.209***	-0.198***
	(0.0202)		(0.050)	(0.005)	(0.066)	(0.069)
Ln GDP pc^2	-0.0067***		0.001		0.011***	0.010**
	(0.0012)		(0.003)		(0.004)	(0.004)
Constant	-0.2607***	-0.024	0.190	0.103*	0.828***	0.784***
	(0.0826)	(0.045)	(0.201)	(0.061)	(0.274)	(0.286)
Cell FE	✓	✓	✓	✓	✓	✓
Year FE	✓	✓	✓	✓	✓	✓
Mean dep var	-0.02	-0.02	-0.02	-0.02	-0.02	-0.02
SD dep var	0.19	0.19	0.19	0.19	0.19	0.19
N	378,529	381,052	378,529	378,529	378,529	378,529
R^2 (inclusive)	0.64	0.63	0.64	0.64	0.65	0.65
R^2 (within)	0.02	0.00	0.03	0.02	0.03	0.03

Notes: Outcome is the outmigration rate. T = temperature, P = precipitation. All specifications include cell and year fixed effects. Standard errors in parentheses. Significance: $^{***}p < 0.01$, $^{**}p < 0.05$, $^{*}p < 0.10$.

Table S5: **Regression results to justify the chosen specification.** Same as S3, except with country standard error clustering (Std. Err. Ctry).

	Dep var: Net Migration rate				
	(1)	(2)	(3)	(4)	(5)
	Climate-Only	Income Quadratic	Quad + Income	Full Interactions	Full Interactions + P^2
T	0.002	0.002	0.014	-0.096*	-0.101**
	(0.008)	(0.022)	(0.010)	(0.055)	(0.050)
T × Ln GDP pc		0.001	-2.34E-04	0.027**	0.029**
		(0.006)	(0.001)	(0.013)	(0.012)
T × Ln GDP pc^2		-1.23E-05		-0.002**	-0.002**
		(3.44E-04)		(0.001)	(0.001)
T^2	2.91E-05		-4.65E-04	0.003	0.003*
	(2.05E-04)		(2.97E-04)	(0.002)	(0.002)
T^2 × Ln GDP pc			3.21E-05	-0.001*	-0.001**
			(2.86E-05)	(4.29E-04)	(3.93E-04)
T^2 × Ln GDP pc^2				5.01E-05*	5.21E-05**
				(2.58E-05)	(2.38E-05)
P	-0.001	-0.053**	-0.003	-0.050**	-0.033
	(0.001)	(0.024)	(0.003)	(0.024)	(0.053)
P × Ln GDP pc		0.013**	2.37E-04	0.012**	0.008
		(0.006)	(3.57E-04)	(0.006)	(0.013)
P × Ln GDP pc^2		-0.001**		-0.001**	-4.45E-04
		(3.50E-04)		(3.50E-04)	(0.001)
P^2					-0.001
					(0.002)
P^2 × Ln GDP pc					1.64E-04
					(4.39E-04)
P^2 × Ln GDP pc^2					-9.76E-06
					(2.64E-05)
Ln GDP pc		-0.038	-0.027***	-0.209	-0.198
		(0.120)	(0.010)	(0.131)	(0.143)
Ln GDP pc^2		0.001		0.011	0.010
		(0.007)		(0.008)	(0.009)
Constant	-0.024	0.190	0.103	0.828	0.784
	(0.082)	(0.472)	(0.107)	(0.536)	(0.589)
Cell FE	✓	✓	✓	✓	✓
Year FE	✓	✓	✓	✓	✓
Mean dep var	-0.02	-0.02	-0.02	-0.02	-0.02
SD dep var	0.19	0.19	0.19	0.19	0.19
N	381,052	378,529	378,529	378,529	378,529
R^2 (inclusive)	0.63	0.64	0.64	0.65	0.65
R^2 (within)	0.00	0.03	0.02	0.03	0.03

Notes: Outcome is the outmigration rate. T = temperature, P = precipitation. All specifications include cell and year fixed effects. Standard errors in parentheses are country-clustered (Std. Err. Ctry). Significance: $^{***}p < 0.01$, $^{**}p < 0.05$, $^{*}p < 0.10$.

Table S6: **Regression results using urban locations instead of rural locations.** Each panel regression includes unit and time fixed effects. The input dataset is the same as for the rest of the analysis, except instead of limiting the analysis to only rural locations, we limit the analysis to only non-rural places.

	Dep var: Net Migration rate	
	(1)	(2)
	Urban (unit SE)	Urban (ctry-cluster SE)
T	0.1114**	0.1114
	(0.0520)	(0.0902)
T × log(GDPpc)	-0.0344***	-0.0344
	(0.0127)	(0.0220)
T × log(GDPpc)^2	0.0022***	0.0022*
	(0.0008)	(0.0013)
T^2	-0.0030**	-0.0030
	(0.0015)	(0.0025)
T^2 × log(GDPpc)	0.0009***	0.0009
	(0.0003)	(0.0006)
T^2 × log(GDPpc)^2	-0.0001***	-0.0001*
	(2.10E-05)	(3.60E-05)
P	0.0228	0.0228
	(0.0202)	(0.0210)
P × log(GDPpc)	-0.0056	-0.0056
	(0.0048)	(0.0050)
P × log(GDPpc)^2	0.0003	0.0003
	(0.0003)	(0.0003)
log(GDPpc)	0.3760***	0.3760***
	(0.1042)	(0.1430)
log(GDPpc)^2	-0.0232***	-0.0232***
	(0.0063)	(0.0088)
Constant	-1.3889***	-1.3889**
	(0.4077)	(0.5672)
Cell FE	✓	✓
Year FE	✓	✓
Mean dep var	-0.02	-0.02
SD dep var	0.11	0.11
N	56,958	56,958
R^2 (inclusive)	0.61	0.61
R^2 (within)	0.06	0.06

Notes: Outcome is the outmigration rate. T = temperature, P = precipitation. All specifications include cell and year fixed effects. Standard errors in parentheses. Significance: $^{***}p < 0.01$, $^{**}p < 0.05$, $^{*}p < 0.10$.

Table S7: **Change in climate-induced rural migration counts for select countries in 2050 relative to 2015 under SSP2.** The first two columns show results using SSP2 time-varying income, the second two columns show results with fixed 2015 income.

Country	SSP income out-migration	SSP income in-migration	Fix income out-migration	Fix income in-migration
IND	1046928	20880	64176	28763
ETH	610294	-33350	73681	1661
NGA	79117	135361	-376	-5755
SAU	32022	103641	20656	25177
KEN	27023	77642	26373	4531
AUS	-15539	-136097	9114	65540
ESP	-17238	-108425	18575	29128
PAN	-19662	-10138	902	2391
GRC	-23719	-6173	4540	5130
CHL	-32712	-43427	5363	8200
VNM	-33833	-66434	7404	21263
JPN	-37420	-339126	14183	93575
DEU	-80668	-137234	31661	84938
ARG	-137278	-53088	12703	12771
ZAF	-158157	397546	29133	31600
RUS	-189313	-128725	112925	103160
BRA	-220150	-34642	36234	11749
MEX	-230572	-83818	37641	36636
USA	-309998	-833193	139865	431925
CHN	-2910065	-58448	819008	22084